

Chapter 1

**Towards Understanding and Applying Stereocontrol in C_1 Symmetric
Metallocene Olefin Polymerization Catalysts Using Group 4 and Group 3
Model Complexes**

Abstract

In order to probe the stereodirecting ability of the $\text{Me}_2\text{Si}(\eta^5\text{-C}_5\text{H}_4)(\eta^5\text{-3-CMe}_3\text{-C}_5\text{H}_3)$ (tBuSp) ligand in propylene polymerization catalysis, we have prepared a series of neutral and cationic group 4 and neutral group 3 model complexes: tBuSpZrCl₂ (**1**), tBuSpZr(CH₂SiMe₃)₂ (**8**), tBuSpZrMe₂ (**9**), [tBuSpZrH₂]₂ (**10**), tBuSpZrMeCl (**11**), tBuSpZrMe(CH₂CMe₃) (**12**), tBuSpZrMe(CH₂SiMe₃) (**13**), tBuSpScCl(THF) (**14**), tBuSpScCH(SiMe₃)₂ (**17**), [tBuSpScH] (**18**), and tBuSpTiCl₂ (**19**). The identities of the kinetically preferred isomers of **12** and **13** have been identified using NOE difference NMR spectroscopy, and in both cases the *syn* isomer, in which the bulky alkyl group is on the same side of the metallocene wedge as the tBu group, is preferred. We have obtained solid state structures of [tBuSpZrH₂]₂ (**10**), tBuSpZrMeCl (**11**), tBuSpZrMe(CH₂CMe₃) (**12**), and tBuSpScCl(THF) (**14**). Complex **10** reacts with D₂ very slowly to form **10-d₄** over six days. Complex **10** also reacts with 2 equivalents of PMe₃ slowly at room temperature to form an equilibrium mixture of tBuSpZrH₂(PMe₃) (**20**), **10**, and PMe₃, with $K_{\text{eq}} = 7.4 \times 10^{-2}$. Complex **10** reacts slowly to insert α -olefins, indicating the relative stability of this complex in its dimeric form. Although we observe a variety of kinetic mixtures of isomers of **12** and **13**, these complexes undergo isomerization in solution in the presence of salts to form predominantly the *anti* isomers, in which the bulky alkyl group is on the opposite side of the metallocene wedge from the tBu substituent on the cyclopentadienyl ring. By identifying the ratio of isomers formed when a methide is abstracted from **9** by B(C₆F₅)₃ to make [tBuSpZrMe]⁺[MeB(C₆F₅)₃]⁻ (**21**), we find that the tBuSp ligand directs a bulky anion to the side of the metallocene wedge away from the tBu substituent *versus* a methyl group fairly well, with a ΔG° of 0.89 kcal/mol at room temperature. Finally, by examining methide abstraction from **13** by B(C₆F₅)₃ to form two isomers of [tBuSpZrCH₂SiMe₃]⁺[Me B(C₆F₅)₃]⁻ (**22**), we find that the tBuSp ligand does not distinguish very well between a bulky anion and a bulky alkyl group in the metallocene wedge ($\Delta G^\circ = 0.27$ kcal/mol). These results suggest that the tBu group is not a very effective

stereodirector in the ground state structures of these metallocenes. Thus the remarkable stereodirecting capability of this ligand must be reconciled by its effect on transition state energies.

Introduction

Since the discovery of α -olefin polymerization by Ziegler and Natta in the 1950's,¹ there has been a great deal of academic and industrial interest in this process.² Current annual worldwide production of polyolefins exceeds 132 billion pounds, and 7 billion pounds of polypropylene are produced in the United States per year.³ Important factors that determine the macroscopic properties of polypropylene are polymer molecular weight and polymer microstructure. The discovery of metallocene complexes that act as single-site, homogeneous catalysts for the polymerization of α -olefins has allowed for the production of polyolefins with high molecular weights and narrow molecular weight distributions, as well as well-defined microstructures. These catalysts have also provided an opportunity to study the mechanism and active species in these polymerizations.

Metallocene catalysts display a well-defined correlation between ancillary ligand structure and polymer stereochemistry. For example, it is known that achiral metallocenes, such as those of C_{2v} symmetry, produce exclusively atactic polypropylene, in which the methyl groups on the backbone are oriented randomly with respect to one another. Alternatively, chiral C_2 symmetric metallocenes produce isotactic polypropylene, in which the methyl groups on the backbone are oriented the same as one another.⁴ Finally, a class of C_s symmetric metallocenes produces syndiotactic polypropylene, in which the methyl groups on the backbone are oriented opposite of each of their neighbors. Examples of these catalysts and the polypropylene they produce are shown in Figure 1.

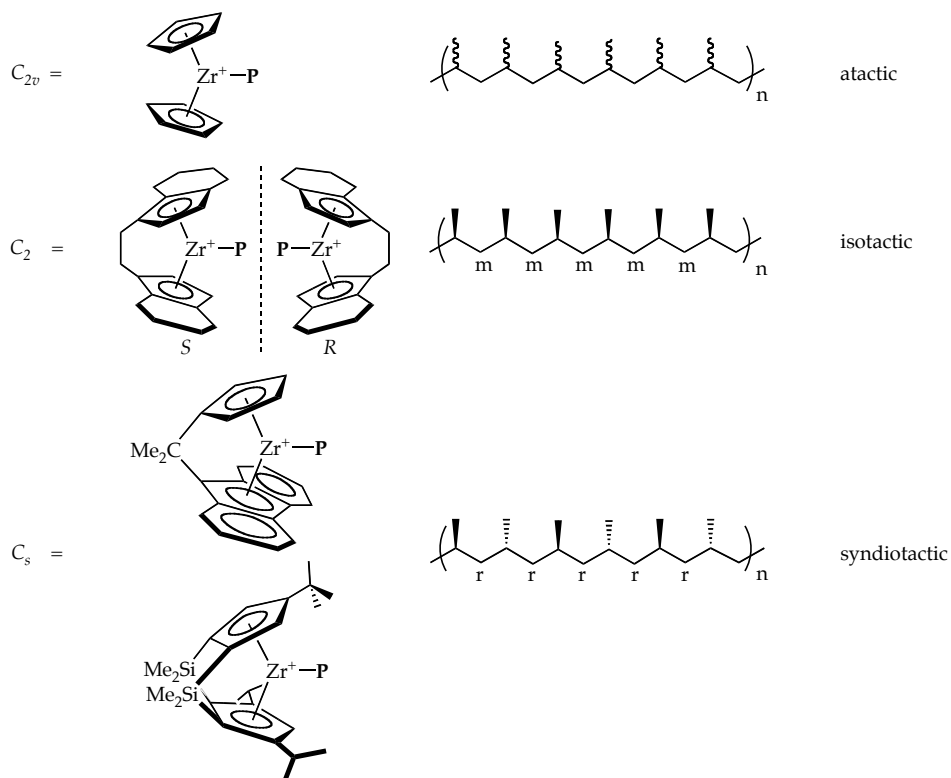


Figure 1. Polypropylene microstructures correlate with catalyst ligand array in a well-defined fashion.

Based on calculations and experimental results, a general model for the interactions that dictate stereocontrol in C_2 and C_s symmetric metallocenes has been developed. In the case of a C_2 symmetric metallocene, the two sides of the metallocene wedge are homotopic. Therefore, the same enantioface of the monomer is inserted, regardless of the side of the wedge where the polymer chain lies. On the other hand, in the case of a C_s symmetric metallocene, the two sides of the wedge are enantiotopic, and insertions occur from alternating sides of the wedge leading to incorporation of opposite enantiofaces of the olefin. Schematic diagrams of the generally accepted transition states for olefin insertions for these classes of metallocenes are shown in Figure 2.

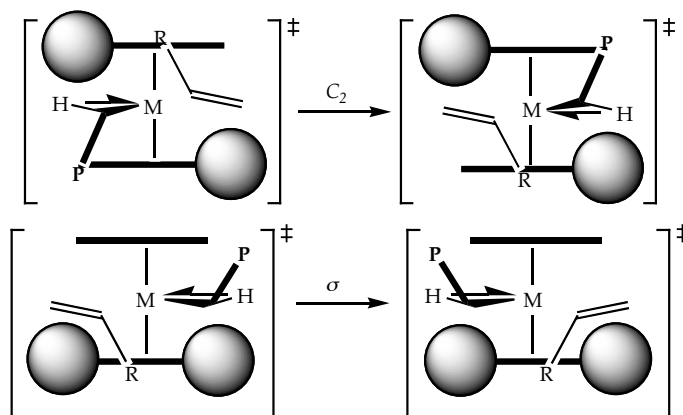


Figure 2. Transition states for olefin insertion for C_2 (top) and C_s (bottom) symmetric catalysts.

Because α -olefin polymerizations operate under kinetic control,⁵ understanding the key steric interactions in the transition state for olefin insertion has been the focus of many theoretical and experimental investigations. It is the relative orientation of the incoming monomer with respect to the polymer chain during this transition state that determines the ultimate tacticity of the polymer. It has been well established that the active species in metallocene-catalyzed α -olefin polymerizations are 14-electron, d^0 metallocene alkyl complexes. These species can either be group 4 metallocene alkyl cations with non-coordinating anions or neutral group 3 metallocene alkyl complexes. These complexes are isoelectronic, and both possess two vacant orbitals. It has been established that in the transition state for olefin insertion,⁶ one of these orbitals is used to accommodate the incoming olefin, and the other orbital allows for an α -agostic interaction, which increases carbon-carbon orbital overlap during bond formation.⁷ Calculations by Corradini demonstrate that the enantiofacial approach of the olefin is determined by the orientation of the metal alkyl unit (or the growing polymer chain), such that the α -substituent on the olefin is placed in a *trans* relationship with respect to the β -carbon of the polymer chain.⁸ The polymer chain is believed to orient toward the most open part of the metallocene wedge. This arrangement is shown in Figure 3.

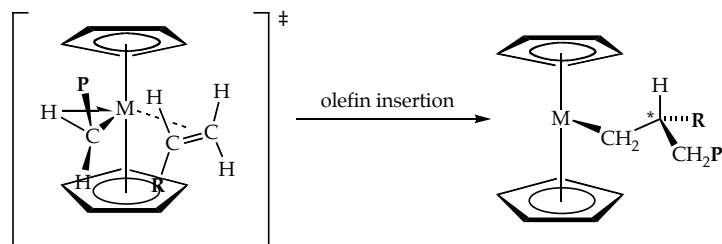


Figure 3. The transition state for olefin insertion in metallocene-catalyzed α -olefin polymerization (**P** = polymer chain, **R** = alkyl), in which the alkyl group on the incoming monomer is oriented *trans* with respect to the polymer chain.

Experimental work to try to elucidate the nature of the important steric interactions during α -olefin insertion began in the late 1980's. The first experimental evidence in support of the calculated model was provided by Pino.⁹ Hydrooligomerization of α -olefins with optically pure [ethylenebis(4,5,6,7-tetrahydroindenyl)]zirconium dichloride ((EBTHI)ZrCl₂) activated with methylaluminoxane (MAO) produces chiral hydrotrimers and hydrotetramers with absolute configurations predicted by the insertion model described above.¹⁰

More recent work carried out in our laboratories compared the relative enantiofacial selectivity for α -olefin insertion into a metal-hydrogen bond *versus* a metal-alkyl bond for a single component ytrocene catalyst that is known to produce highly isotactic polypropylene.¹¹ Using an optically pure, isotopically chiral 1-pentene the selectivity for insertion into the yttrium-hydrogen bond was determined to be relatively low (34% ee), while the selectivity for insertion into the yttrium-alkyl bond is greater than 40:1. These results suggest that while direct interactions between the metallocene ligand and the olefin do not provide very good stereodirection, interactions between the ligand and the polymer chain and between the polymer chain and the incoming monomer can impart very high stereoselectivity on insertion reactions.

This experiment has allowed us to gain an understanding of the important interactions that dictate stereocontrol. We conclude that in the transition state for olefin insertion, the ligand array directs the polymer chain and the polymer chain directs the monomer to be oriented in a *trans* arrangement with respect to the polymer chain (Figure 3). This type of stereocontrol, in which the steric interactions between the catalyst and the polymer dictate enantiofacial selectivity for olefin insertion, is called enantiomorphic site control.

While for the symmetric catalysts shown in Figure 1 the effect of ligand array on polymer stereochemistry is well understood, for other, less symmetric catalysts, the way in which the ancillary ligand determines the microstructure of polypropylene has not been well characterized. It is known that a class of sterically open C_1 symmetric metallocenes makes isotactic polypropylene.¹² Specifically, $\text{Me}_2\text{Si}(\eta^5\text{-C}_5\text{H}_4)(\eta^5\text{-3-(CMe}_3\text{)-C}_5\text{H}_3)\text{ZrCl}_2$ (tBuSpZrCl₂, **1**) produces moderately isotactic polypropylene when activated with MAO ([mmmm] = 77.9%).^{12a} It is clear that the tBuSp ligand has remarkable stereodirecting capability, but the origin of this stereocontrol is not obvious. Based on the previously discussed models it is reasonable to suggest three possible transition state geometries for olefin insertion, as shown in Figure 4. Insertions from the transition state structure in which the polymer chain is on the same side of the metallocene wedge as the tBu group (Figure 4A) are expected to be more stereospecific based on our model for enantiomorphic site control, as this structure closely resembles the picture of a C_2 symmetric catalyst. It is possible that the polymer chain undergoes facile site epimerization after insertion, and insertions occur primarily from this more stereoselective transition state. Insertions from the transition state structures in which the polymer chain is on the opposite side of the metallocene wedge from the tBu group (Figure 4B) would produce stereoerrors.

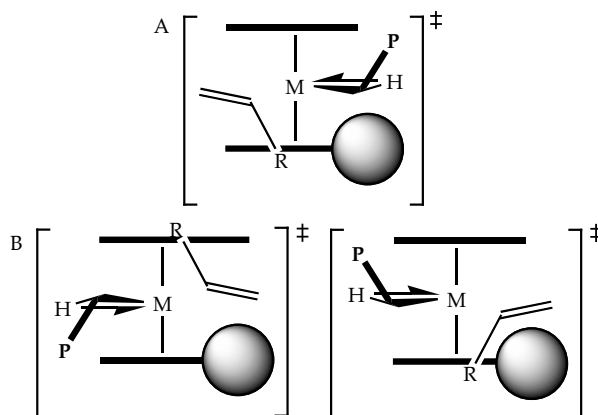


Figure 4. Possible transition states for olefin insertion for catalyst **1**. A. The more stereoselective transition state. B. The less stereoselective site where stereoerrors may occur.

Polymerization studies have been carried out using **1** activated by MAO under different conditions to try to probe the origin of the stereoselectivity observed for this catalyst. The stereoregularity of polymers made with **1** does not vary significantly with monomer concentration or polymerization temperature, which indicates that for this catalyst site epimerization is fast relative to monomer enchainment.^{12b} Thus the monomer is preferentially inserted at the more stereoselective site more frequently to give highly isotactic polymer.

Studies of group 5 metallocene olefin hydride complexes, whose ground states may serve to model transition states for olefin insertions during metallocene-catalyzed α -olefin polymerizations,¹³ also indicate that the tBuSp ligand has remarkable stereodirecting capability. In fact, for both tBuSpNb(styrene)(H) (**2**) and tBuSpTa(styrene)(H) (**3**), only one isomer of the complexes is observed both in solution and in the solid state.^{13c} The isomer observed is the one in which the styrene is coordinated *endo* in the metallocene wedge on the opposite side of the wedge from the tBu group, with the phenyl group pointed away from the tBu group, as shown in Figure 5.

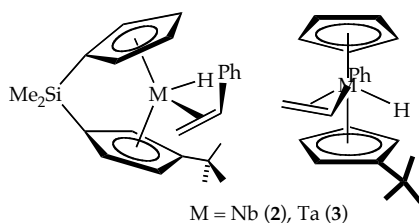


Figure 5. Side and front view of the only isomer observed for tBuSpM(styrene)(H) complexes **2** and **3**.

Based on the polymerization results, as well as the results of the studies of group 5 model complexes, we set out to gain a better understanding of the factors that dictate stereocontrol in these C_1 symmetric systems, as well as to design complexes to apply this remarkable stereocontrol to enantioselective reactions. We prepared neutral and cationic zirconocene complexes to gain insight into the interaction between the ligand array and zirconium alkyl groups, as well as the relative ability of the ligand array to direct a bulky anion *versus* a bulky alkyl group of the active species. We also prepared neutral scandocene and yttrocene complexes of the tBuSp ligand. Concurrently we prepared the analogous titanocene complex in an effort to apply the observed stereocontrol to catalytic enantioselective hydrosilylation of trisubstituted olefins.

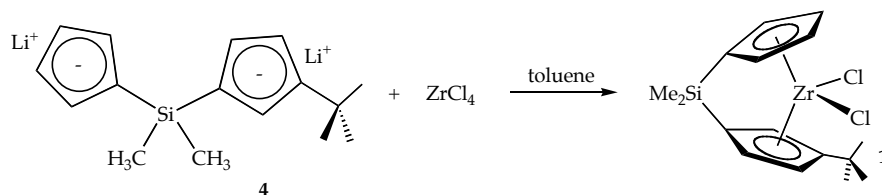
Results and Discussion

Synthesis and Characterization of tBuSp Complexes of Zirconium

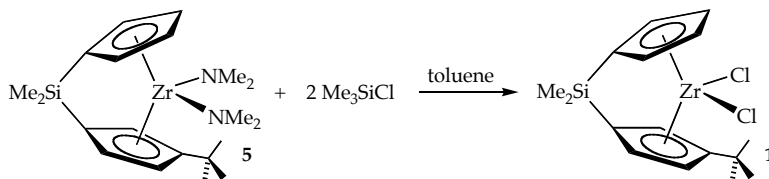
Synthesis of complex **1** may be accomplished using two different routes. Reaction of the dilithio salt of the tBuSp ligand (Li_2tBuSp , **4**) with $ZrCl_4$ in refluxing toluene for five days, followed by recrystallization of the product from diethyl ether, provides **1** as a tan powder in 55% yield (Scheme 1). This complex displays seven distinct 1H NMR resonances in benzene- d_6 at room temperature for the seven inequivalent protons on the cyclopentadienyl rings of the tBuSp ligand, a single resonance for the tBu group, and two resonances for the inequivalent dimethylsilyl protons. Because it is often

difficult to separate **1** from LiCl, it was desirable to find another route for preparation of **1**. Alternatively, tBuSpZr(NMe₂)₂ (**5**) can be prepared via an amine elimination reaction, according to the method of Jordan,¹⁴ by refluxing Zr(NMe₂)₄ (**6**) with the protio tBuSp ligand (tBuSpH₂, **7**) in toluene. The reaction of **5** with Me₃SiCl in toluene (Scheme 2), again following methodology developed by Jordan,¹⁴ produces **1** in 58% isolated yield.

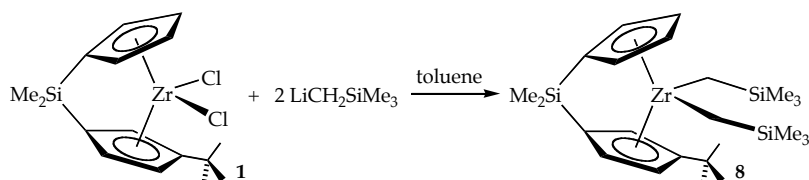
Scheme 1.



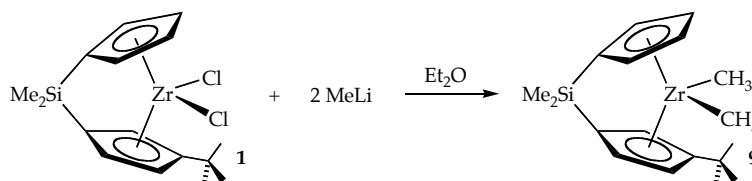
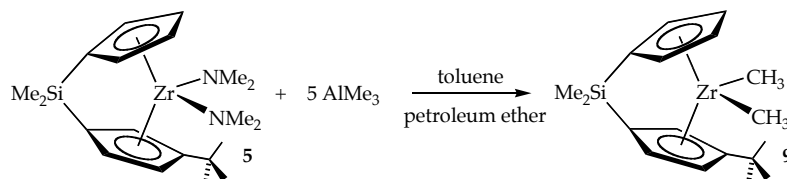
Scheme 2.



The dialkyl complex tBuSpZr(CH₂SiMe₃)₂ (**8**) can be prepared from the reaction of **1** with 2 equivalents of LiCH₂SiMe₃ in toluene (Scheme 3). Although ¹H NMR shows that **8** is formed in high yield (> 80%), due to its high solubility, it is isolated as an orange powder in only 5% yield by recrystallization from petroleum ether. Because it is C₁ symmetric, its ¹H NMR spectrum exhibits seven distinct peaks for each of the cyclopentadienyl protons, two distinct resonances for the dimethylsilyl groups, two distinct resonances for the trimethylsilylmethyl groups, as well as characteristic peaks for each of the diastereotopic protons of the methylene groups of the trimethylsilylmethyl groups.

Scheme 3.

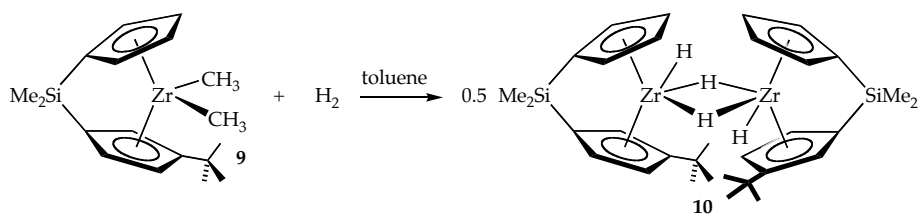
Isolation of tBuSpZrMe₂ (**9**) can be accomplished using two different routes. The reaction of **1** with methyllithium in diethyl ether affords **9** as an off-white powder in 42% yield (Scheme 4). Reaction of **5** with 5 equivalents of AlMe₃ in a mixture of toluene and petroleum ether, according to the method of Jordan,¹⁴ provides **9** in 47% yield (Scheme 5).

Scheme 4.**Scheme 5.**

The dihydride complex [tBuSpZrH₂]₂ (**10**) can be prepared by hydrogenation of **9** in toluene for 14 days (Scheme 6), according to the procedure reported for the synthesis of metallocene dihydride complexes of the general form [Cp*(R_nCp)ZrH₂]_n (Cp* = pentamethylcyclopentadienyl; R_nCp = substituted cyclopentadienyl; n = 1, 2).¹⁵ This reaction proceeds via σ bond metathesis of the Zr-CH₃ with H₂. Complex **10** can be isolated as a white powder in 47% yield by recrystallization from cold petroleum ether. It is possible to determine the nuclearity of **10** in solution using ¹H NMR spectroscopy. While monomeric zirconium dihydrides exhibit a single downfield resonance ($\delta \approx 7$ to 8), dimeric zirconocene dihydrides display separate resonances for terminal ($\delta \approx 4$ to 5) and bridging hydrides ($\delta \approx -1$ to

1).¹⁵ Complex **10** displays two hydride resonances in benzene- d_6 at room temperature, one triplet at $\delta = 4.13$ ppm and another triplet at $\delta = -2.05$ ppm, indicating that it is a dimer in solution at room temperature. Complex **10** displays a single room temperature ^1H NMR resonance for the tBu group at $\delta = 1.49$ ppm, two distinct peaks for the dimethylsilyl groups, as well as seven distinct resonances for the protons on the cyclopentadienyl rings.

Scheme 6.



Cooling a saturated toluene solution of **10** to -30 °C affords colorless crystals suitable for X-ray diffraction. The solid state structure of **10** has been obtained, and it is shown in Figures 6 and 7. Unlike all of the previously characterized zirconocene dihydride dimers, complex **10** does not contain a center of symmetry in the solid state.¹⁶ Both tBu groups are on the “bottom” of the metallocene wedge, but they are oriented *trans* to one another. The dihedral angle of 63.1 degrees between the two zirconocene cyclopentadienyl-centroid vectors presumably alleviates unfavorable steric interactions between the two tBu substituents. The solid state structure of **10** is consistent with the number of peaks observed in the room temperature ^1H NMR spectrum. The distance of 3.3704(4) Å between the two zirconiums is slightly shorter than other crystallographically characterized zirconocene dihydride dimers, which display zirconium-zirconium distances of 3.4-3.5 Å.¹⁶

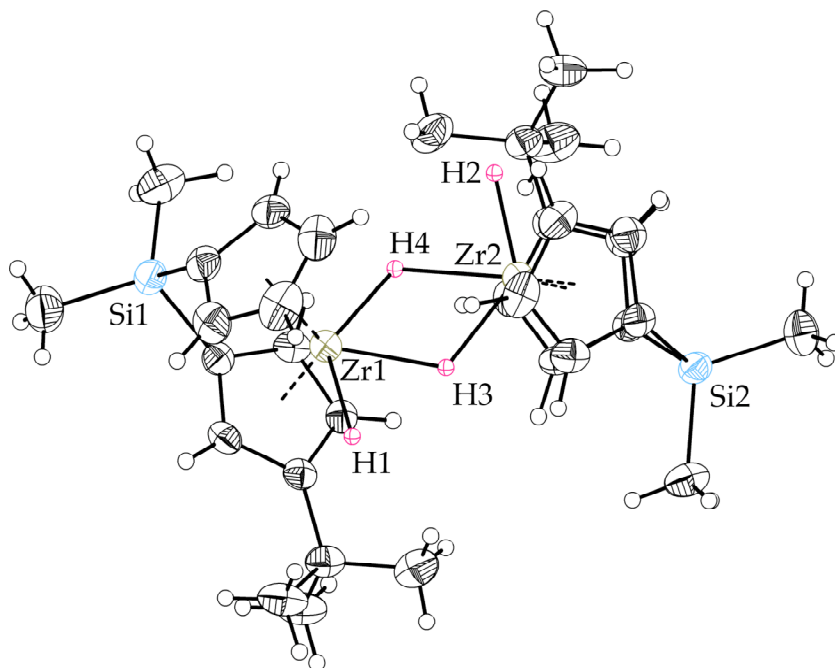


Figure 6. Top view of **10** with 50% probability ellipsoids.

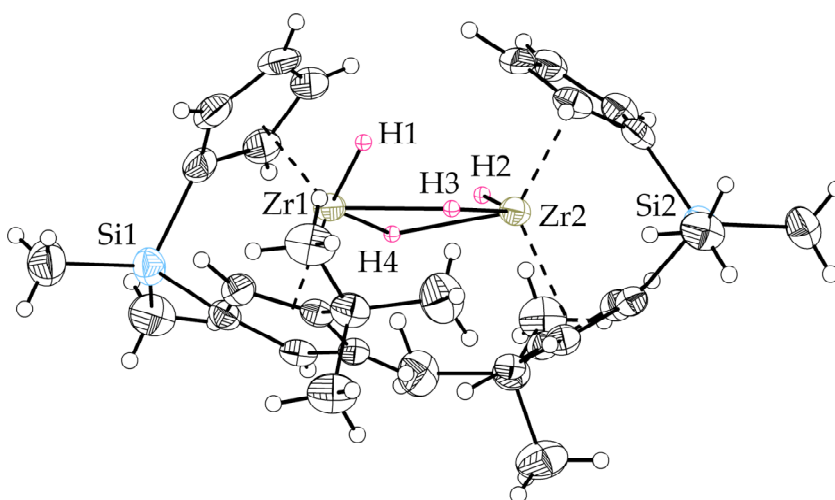


Figure 7. Side view of **10** with 50% probability ellipsoids.

All four of the zirconium-hydrides were located in the difference map and have been refined isotropically. The zirconium-hydride bond lengths are listed in Table 1. It is very doubtful that the apparent large difference between the zirconium-hydride bond lengths for the terminal hydrides (Zr(1)-H(1) and Zr(2)-H(2)) is real. However, the shorter distance to the bridging hydride *cis* to the terminal hydride as compared to the *trans*

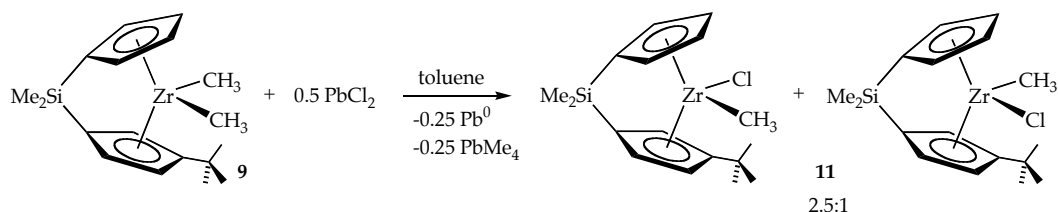
bridging hydride distance (e.g., Zr(1)-H(3) *versus* Zr(1)-H(4)) for a given zirconium may be meaningful.

Bond	Bond Length (Å)
Zr(1)-H(1)	2.00(2)
Zr(1)-H(3)	1.83(2)
Zr(1)-H(4)	2.01(2)
Zr(2)-H(2)	1.76(2)
Zr(2)-H(3)	2.05(2)
Zr(2)-H(4)	1.92(2)

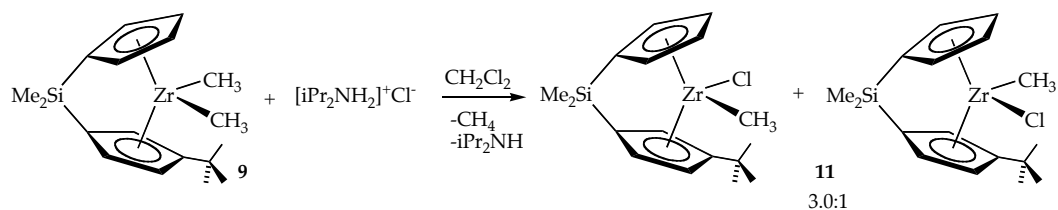
Table 1. Zirconium-hydride bond lengths for terminal and bridging hydrides in **10**.

Synthesis of tBuSpZrMeCl (**11**) can be accomplished by three different routes. In all cases **11** is formed as mixtures of two isomers, which seems reasonable as methyl and chloride are sterically similar. Reaction of **9** with 0.5 equivalents of PbCl₂ in benzene-*d*₆ for 72 hours gives **11** as a 2.5:1 mixture of isomers, one in which the chloride is *syn* to the tBu group and the other in which the chloride is *anti* to the tBu group (Scheme 7). However, we have not identified the stereochemistry of the two isomers by NOE difference NMR spectroscopy. Alternatively, the reaction of [iPr₂NH₂]⁺Cl⁻ with **9** in dichloromethane over 18 hours provides 69% yield of a 3.0:1 mixture of the two isomers of **11** (Scheme 8). Finally, the conproportionation reaction between **1** and **9** in toluene at 80 °C for five days affords **11** in 57% isolated yield as a 2.7:1 mixture of the two possible isomers (Scheme 9). The thermodynamically preferred ratio of these two isomers has not been determined.

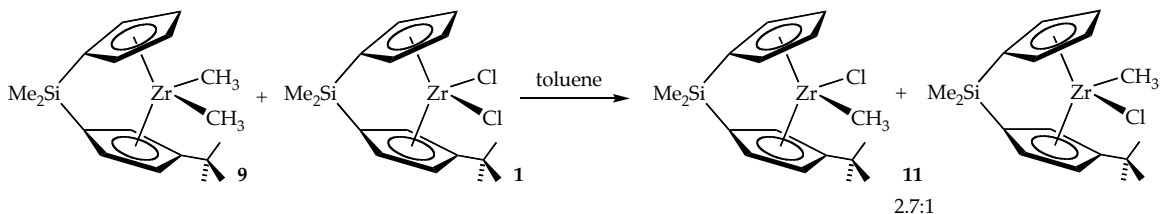
Scheme 7.



Scheme 8.



Scheme 9.



Cooling a saturated solution of **11** in hexanes provides yellow crystals that are suitable for X-ray diffraction. The solid state structure of **11** has been obtained, and it is shown in Figure 8. Compound **11** crystallizes predominantly as the isomer with chloride *syn* to the *t*Bu group. However, there is some disorder in the crystal, as the methyl site appears to contain chloride approximately 35% of the time, while the chloride site may contain methyl significantly less than 35% of the time. This suggests that the compound crystallizes as a mixture of **11** and **1**, as well as with some disorder due to the presence of both isomers of **11**. The zirconium-methyl bond length of 2.23(2) Å is on the short end of the range of 2.24-2.40 Å for zirconium-carbon bonds amongst $(\text{R}_n\text{Cp})_2\text{Zr}(\text{R})\text{Cl}$ complexes.¹⁷ Additionally, it is shorter than the zirconium-methyl bond of 2.361 Å in Cp_2ZrMeCl .¹⁸ The zirconium-chloride bond length of 2.4542(13) Å is within the range of 2.42-2.57 Å for zirconocene alkyl chloride complexes,¹⁹ and it is quite close to the zirconium-chloride bond of 2.487 Å for Cp_2ZrMeCl .¹⁸ The zirconium-chloride bond length for the chloride in the methyl site is 2.413(7) Å.

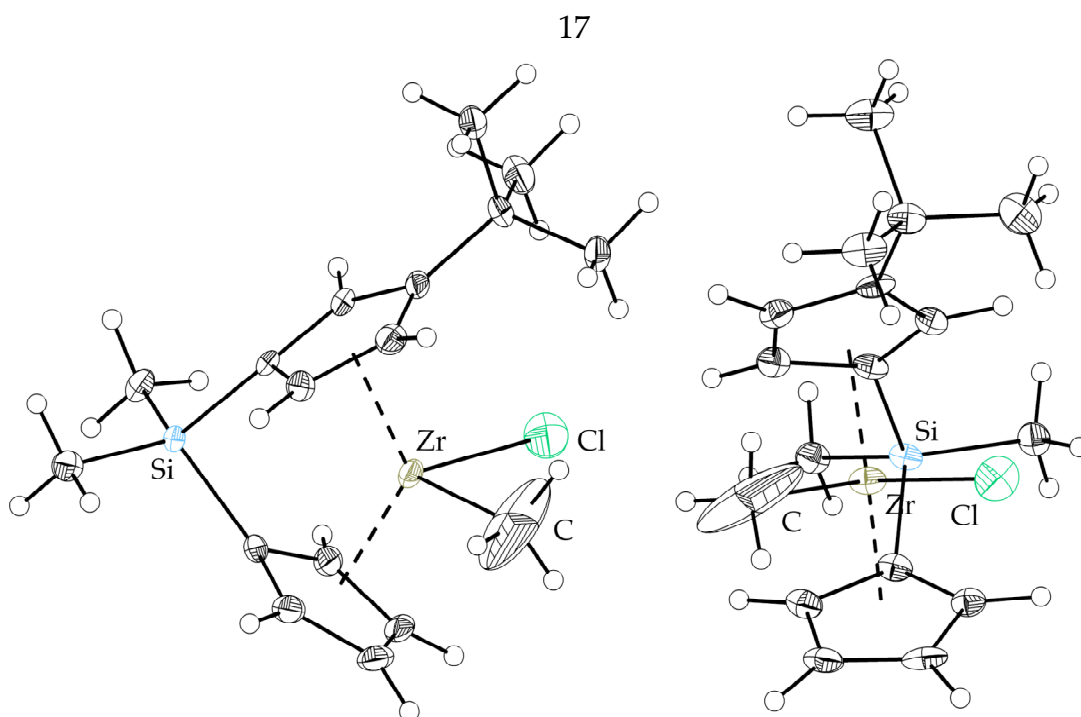
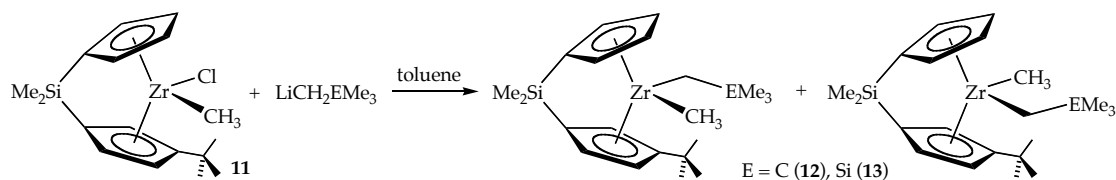


Figure 8. Side and front view of **11** with 50% probability ellipsoids.

Preparation of $t\text{BuSpZrMe}(\text{CH}_2\text{CMe}_3)$ (**12**) and $t\text{BuSpZrMe}(\text{CH}_2\text{SiMe}_3)$ (**13**) proceeds from the reaction of **11** with the corresponding lithium alkyl reagent ($\text{LiCH}_2\text{CMe}_3$ or $\text{LiCH}_2\text{SiMe}_3$) in toluene, as shown in Scheme 10. In all cases a mixture of isomers of these complexes is observed in solution by ^1H NMR spectroscopy. The two isomers for each compound have been identified by NOE difference NMR spectroscopy at room temperature, and for both **12** and **13** we observe that the kinetically preferred isomer is the *syn* isomer, in which the bulky alkyl group is on the same side of the wedge as the *t*Bu group. Irradiation of the *t*Bu group of the major isomer of **12** provides strong NOE enhancement of one of the methylene protons of the neopentyl group. Irradiation of one of the diastereotopic methylene protons of the major isomer of **13** affords a strong NOE enhancement of the *t*Bu group on the ligand, as well as weaker enhancement of the other methylene proton, the SiMe_3 group, and the zirconium-methyl group of the major isomer. Irradiation of the *t*Bu groups of both isomers gives NOE enhancement of the methylene protons of the major isomer, as well as strong enhancement of the zirconium-methyl protons of the minor isomer.

Scheme 10.



Depending on the exact reaction conditions and reaction time, different kinetic product mixtures are isolated for **12** and **13**. In the case of **12**, the kinetic product can be isolated as a 1.2-3.4 to 1 mixture of the isomer containing the neopentyl group *syn* to the tBu group and the isomer with the methyl group *syn* to the tBu group. The kinetic product for **13** is a 1.3-2.0 to 1 mixture of these analogous isomers.

The solid state structure of **12** has been obtained and is shown in Figure 9. Cooling a saturated hexanes solution of **12** provides crystals suitable for X-ray diffraction. Complex **12** crystallizes as the isomer with the neopentyl group *syn* to the tBu group. The zirconium-methyl distance is 2.274(4) Å and the zirconium-methylene distance is 2.247(4) Å. These distances are within the normal range for zirconocene-carbon distances for zirconocene-dimethyl and zirconocene-dialkyl complexes.²⁰

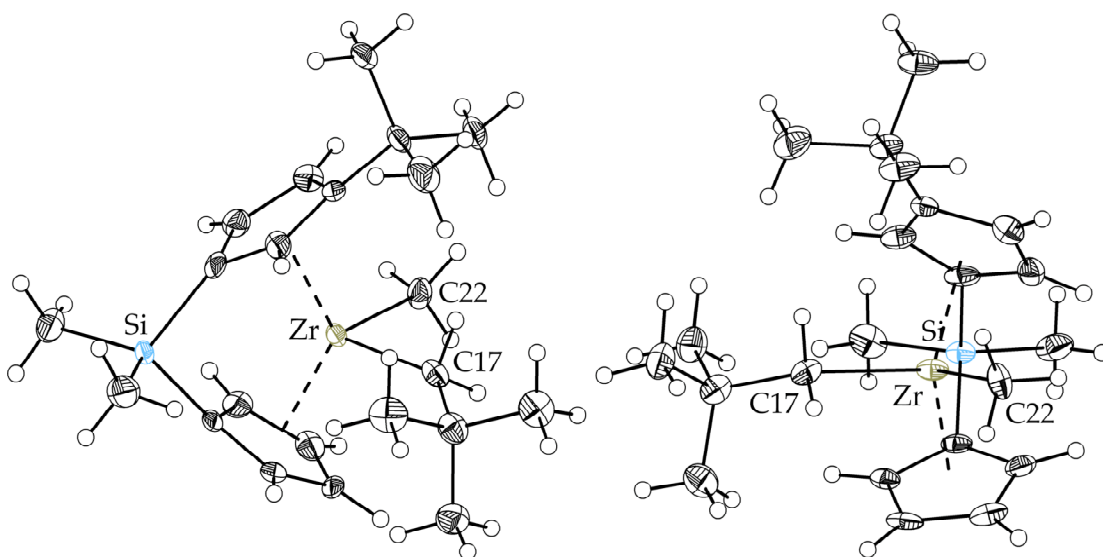
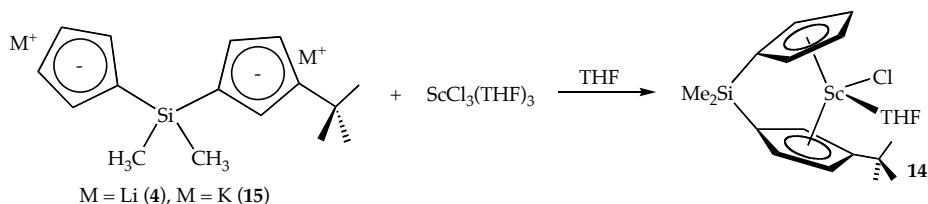


Figure 9. Side and front view of **12** with 50% probability ellipsoids.

Synthesis and Characterization of tBuSp Complexes of Scandium and Yttrium

Synthesis of tBuSpScCl(THF) (**14**) may be accomplished by reaction of either **4** or the dipotassium salt of the tBuSp ligand (K₂tBuSp, **15**) with ScCl₃(THF)₃ in THF, as shown in Scheme 11. Complex **14** has been isolated from the reaction with **15** as an off-white powder in 40% yield by recrystallization from petroleum ether. In all cases only a single isomer of the product is observed by ¹H NMR at room temperature in THF-*d*₈ solution. The analogous yttrium complex, [tBuSpYCl] (**16**), may be prepared from **15** and YCl₃(THF)₃.

Scheme 11.



The solid state structure of **14** has been obtained and is shown in Figure 10. Cooling a saturated diethyl ether solution of **14** provides colorless crystals suitable for X-ray diffraction. The structure displays only the isomer in which the chloride is *syn* to the tBu group on the ligand. The scandium-chloride bond length is 2.4462(6) Å, and the scandium-oxygen bond length is 2.2071(13) Å. There is only one other known structurally characterized scandocene THF complex, Cp₂ScSi(SiMe₃)₃(THF), which has a scandium-oxygen bond length of 2.217 Å.²¹

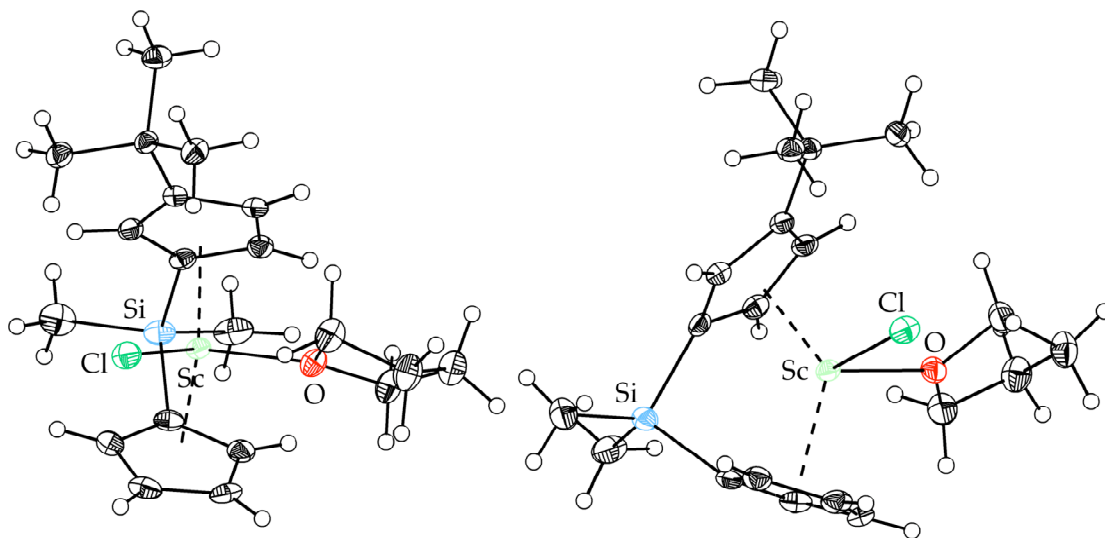
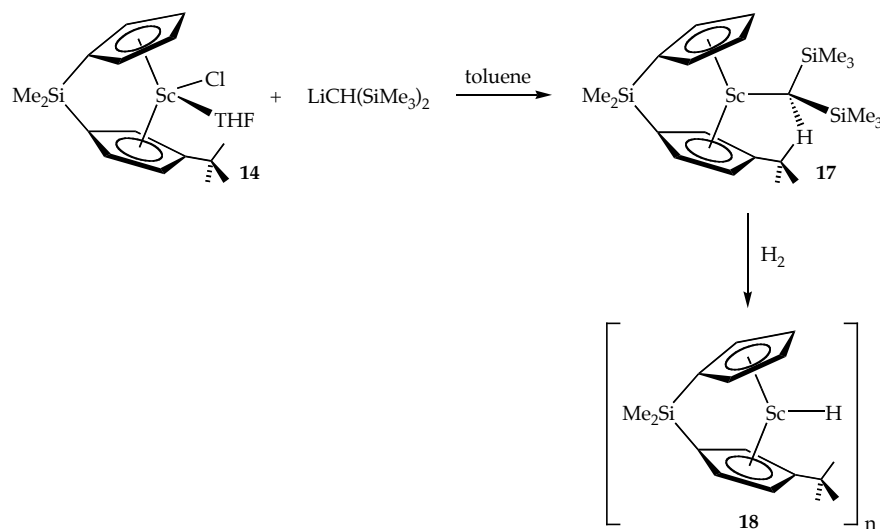


Figure 10. Molecular structure of **14** with 50% probability ellipsoids.

Preparation of $t\text{BuSpScCH}(\text{SiMe}_3)_2$ (**17**) can be accomplished by alkylation of **14** with $\text{LiCH}(\text{SiMe}_3)_2$ in toluene (Scheme 12), and **17** is isolated as a yellow oil. This complex exhibits the expected seven peaks for the cyclopentadienyl protons in the ^1H NMR in benzene- d_6 at room temperature, as well as two distinct peaks for each of the dimethylsilyl groups and two peaks for the diastereotopic trimethylsilyl groups. Hydrogenation of **17** with H_2 over 1 week affords $[\text{tBuSpScH}]_n$ (**18**) (Scheme 12). By ^1H NMR we observe seven cyclopentadienyl peaks, a single $t\text{Bu}$ peak, and two dimethylsilyl resonances at room temperature. Observation of a scandium-hydride resonance by ^1H NMR has not been possible, presumably due to the proximity of the hydride to the quadrupolar scandium nucleus. We have not determined the nuclearity of this species; we believe it is a dimer, but the bridging mode has not been established. Two types of hydride-bridged dimers of group 3 and lanthanide *ansa*-metallocenes have been described previously; one type, the “flyover” dimeric structure, involves each linked cyclopentadienyl ligand spanning two metal atoms, and the other involves bridging of the two metal atoms by two hydrides.²²

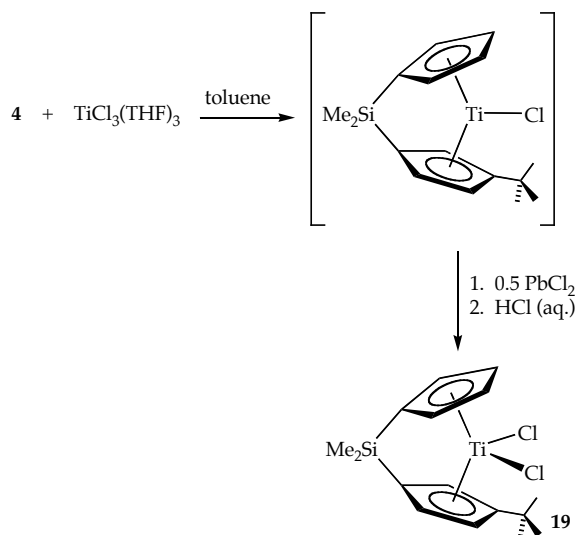
Scheme 12.



Synthesis and Characterization of tBuSp Complexes of Titanium

Synthesis of tBuSpTiCl_2 (**19**) can be accomplished from the reaction of $\text{TiCl}_3(\text{THF})_3$ and **4** in toluene, followed by oxidation of the product, presumably $[\text{tBuSpTiCl}]$, with PbCl_2 and aqueous HCl in air (Scheme 13). The product can be extracted from water with carbon tetrachloride and washed with petroleum ether to obtain pure **19** as a brown powder in 25% yield. EPR spectra of **19** in toluene at room temperature or 77 K do not show the presence of any Ti(III) species.

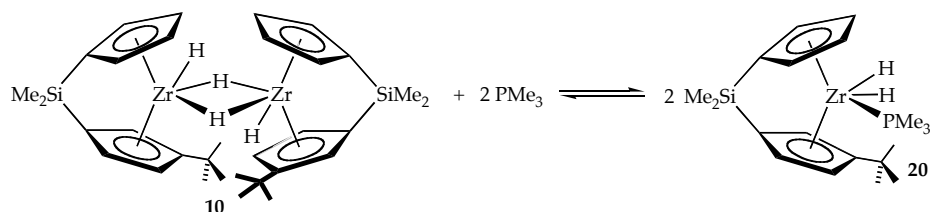
Scheme 13.



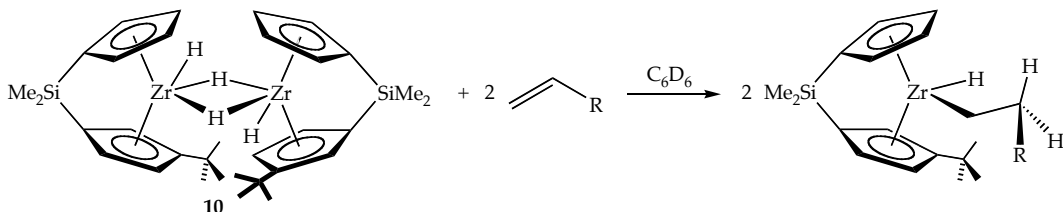
Reactivity of **10**

Complex **10** reacts with D_2 to form $[\text{tBuSpZrD}_2]_2$ (**10-d₄**), presumably via formation of the monomer of **10** followed by σ bond metathesis with D_2 . However, it takes approximately six days for **10** to undergo complete deuterium exchange, which is slow compared to other zirconocene dihydride complexes, indicating that **10** is a relatively stable dimer. Complex **10** reacts with 2 equivalents of PMe_3 to form $\text{tBuSpZrH}_2(\text{PMe}_3)$ (**20**), as shown in Scheme 14. However, at room temperature this reaction has an equilibrium constant of approximately 7.4×10^{-2} , so a mixture of **10**, PMe_3 , and **20** is observed. Reactions of complex **10** with α -olefins, such as styrene and 1-butene, proceed slowly to form the insertion products, $\text{tBuSpZr}(\text{R})(\text{H})$, as shown in Scheme 15. The observed slow reactivity confirms the stability of the dimeric form of **10**, as presumably only the monomeric, 16-electron form of **10** can coordinate and insert olefins.

Scheme 14.



Scheme 15.

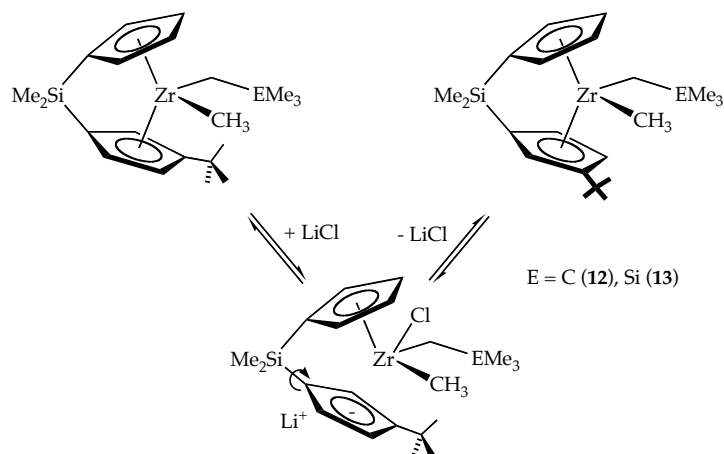


Studies on the Stereodirecting Capability of the tBuSp Ligand

Although **12** and **13** can be isolated as kinetic mixtures of the two possible isomers of these complexes, we observe that solutions of **12** and **13** in the presence of salts isomerize to thermodynamic product mixtures over time. In both cases the thermodynamically preferred isomer is the one in which the bulky alkyl group is on the opposite side of the wedge from the tBu group. For **12**, the thermodynamic ratio of products is greater than 90% in favor of the *anti* isomer, which corresponds to a ΔG° of greater than 1.3 kcal/mol, while for **13** the thermodynamic ratio is approximately 80% in favor of the same isomer, corresponding to a ΔG° of 0.82 kcal/mol.

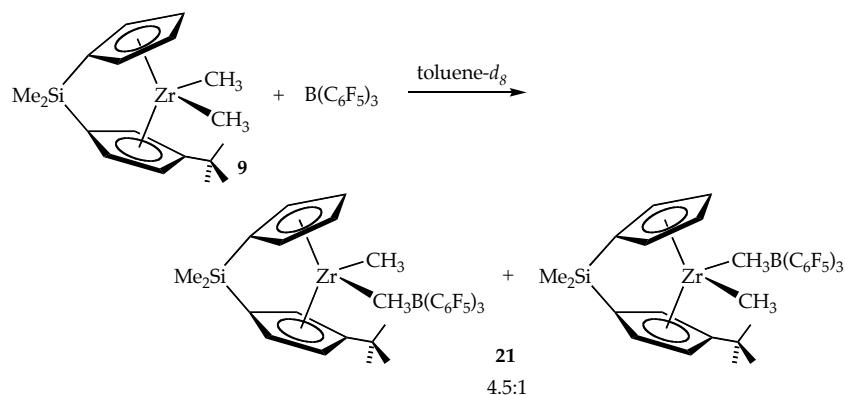
This type of isomerization, which is promoted by salts or coordinating solvents, has been previously observed for scandocene, yttrrocene, and similar lanthanide derivatives, as well as for some zirconocene complexes.²³ We propose that the isomerization proceeds via heterolytic cleavage of the zirconium-cyclopentadienyl bond, followed by rotation around the silicon-carbon bond and recoordination of the cyclopentadienyl to zirconium to form the other isomer, as shown in Scheme 16.

Scheme 16.



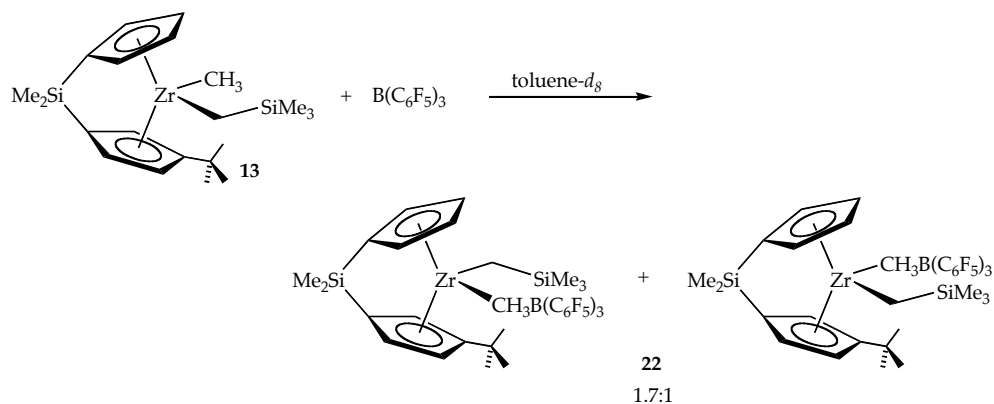
In order to investigate the ability of the tBu group to direct a non-coordinating anion in the metallocene wedge, we examined the isomers formed when a methide is abstracted from **9** by $\text{B}(\text{C}_6\text{F}_5)_3$ to form $[\text{tBuSpZrMe}]^+[\text{MeB}(\text{C}_6\text{F}_5)_3]^-$ (**21**) (Scheme 17). At room temperature in toluene- d_8 , two isomers of **21** are observed in an approximately 4.5:1 ratio, which corresponds to a ΔG° of 0.89 kcal/mol. These isomers undergo slow chemical exchange at room temperature, presumably by the generally accepted mechanism for this process, which involves dissociation of $[\text{MeB}(\text{C}_6\text{F}_5)_3]^-$ from zirconium, followed by recoordination of the anion on the other side of the metallocene wedge.²⁴ We performed NOE difference NMR spectroscopy on this mixture at -20°C in order to identify the two isomers conclusively, as the exchange process does not occur at this temperature. Based on the observed significant enhancement of the zirconium-methyl resonance of the major isomer upon irradiation of the tBu resonance of the same isomer, we have determined that this isomer of **21** is the one in which the anion sits on the opposite side of the wedge from the tBu group. This suggests that the tBu group does direct the anion fairly well in the metallocene wedge. However, the selectivity observed for this model system cannot explain the high isotacticity of the polypropylene produced by **1** activated with MAO.

Scheme 17.



Finally, we have compared the ability of the tBu group to direct a bulky anion *versus* an alkyl group in the metallocene wedge. We have examined the abstraction of methide from **13** by $\text{B}(\text{C}_6\text{F}_5)_3$ in $\text{toluene-}d_8$ at low temperature to produce two isomers of $[\text{tBuSpZrCH}_2\text{SiMe}_3]^+[\text{Me B}(\text{C}_6\text{F}_5)_3]^-$ (**22**), as shown in Scheme 18. These two isomers undergo fast exchange at room temperature, but below $0\text{ }^\circ\text{C}$ it is possible to observe two separate isomers. However, we have not done conclusive NOE difference NMR experiments to assign the two isomers, as the proximity of many of the key ^1H NMR resonances renders selective irradiation of peaks difficult. We have determined the ratio of these two isomers by ^1H NMR integration at different temperatures to be approximately 1.7:1, and we have found that $K_{\text{eq}} \approx 1.7$ from 213 - 273 K, corresponding a ΔG° value of approximately 0.27 kcal/mol. The small ΔG° observed at all temperatures suggests that the tBu group does not differentiate well between the $[\text{Me B}(\text{C}_6\text{F}_5)_3]^-$ anion and the trimethylsilylmethyl group.

Scheme 18.



These results suggest that the tBuSp ligand does not possess remarkable stereodirecting capabilities for complexes that model the ground states for olefin polymerizations. In fact, the tBu group cannot differentiate very well between bulky alkyl groups, which represent models for the growing polymer chain, and a methyl group, between bulky anions and a methyl group, or between bulky anions and bulky alkyl groups. This suggests that, in the ground state prior to olefin insertion, rapid exchange between the groups occupying sites in the metallocene wedge is possible. We extend this finding to suggest that, during olefin polymerizations with these catalysts, site epimerization of the growing polymer chain in the metallocene wedge is rapid. However, we do not know the relative rate of site epimerization *versus* the rate of olefin insertion. If site epimerization is fast compared to olefin insertion, it must be differences between transition state energies that determine the enantiofacial preference for α -olefin insertion. In other words, the transition state for olefin insertion on the more stereoselective side of the metallocene wedge is of lower energy than the transition state for insertion on the other side of the wedge.

A schematic representation of this situation is shown in Figure 11. We use the ΔG° value of 0.27 kcal/mol determined from our study of the site preference of a bulky anion versus a bulky alkyl group in the metallocene wedge in [tBuSpZr]. This conclusion is consistent with our model for enantiomorphic site control, in which interactions between the ligand array

and the polymer chain are most important in determining the stereospecificity of olefin insertions. These conclusions also correlate well with the observed polymerization results discussed in the introduction. Additionally, the results validate the notion that group 5 olefin-hydride complexes can serve as models for the transition states for olefin insertion during polymerization, as we suggest that it is only in the transition state that the tBuSp ligand exerts excellent stereocontrol.

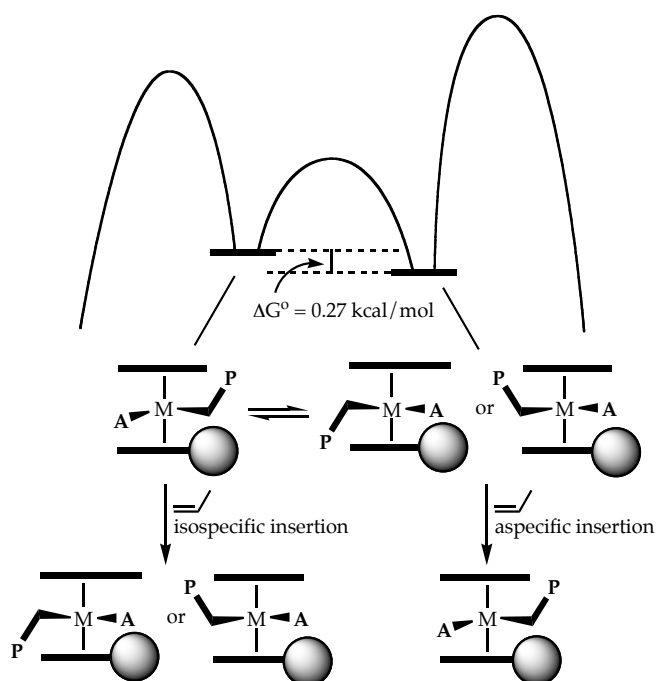


Figure 11. Schematic representation of the low barrier for site epimerization in the ground state structure and the lower barrier for olefin insertion on the more stereoselective side of the metallocene wedge as compared to the barrier for insertion on the less stereoselective side of the wedge (**P** = polymer chain, **A** = anion).

Conclusions

In order to gain insight into the remarkable stereodirecting capability of the tBuSp ligand, a series of group 4 and group 3 complexes of tBuSp have been prepared and characterized by NMR spectroscopy and X-ray

crystallography. Many novel complexes have been isolated. We find that the zirconocene dihydride complex is very stable in its dimeric form. We have obtained an X-ray crystal structure of a scandocene-THF complex, which represents one of only two in this family of complexes.

Our examination of the ability of the tBuSp ligand to direct alkyl groups and an anion in the wedge has lent insight into the mechanism of stereocontrol for this catalyst system. We have examined the ratios of isomers obtained for neutral zirconocene methyl alkyl complexes, in which the alkyl substituent serves as a model for a growing polymer chain attached to the metal. We find that while a variety of kinetic mixtures of isomers are formed for either neopentyl or trimethylsilylmethyl groups, these complexes are able to isomerize to predominantly the isomer in which the bulky alkyl group is *anti* with respect to the tBu substituent on the cyclopentadienyl ring. Additionally we find that the tBu group is able to direct the bulky anion, $[\text{MeB}(\text{C}_6\text{F}_5)_3]^-$, to the opposite side of the wedge fairly well in the case where the other group in the wedge is methyl. However, the tBuSp ligand does not distinguish well between a bulky alkyl group and the bulky anion. These results suggest that the tBu group does not exert very good stereocontrol in models of the ground state for olefin insertion during polymerization. We therefore conclude that this ligand must be a very effective stereodirector in the transition state for olefin insertion. Thus, the active catalyst is able to undergo rapid site epimerization and more frequent insertion from the more stereoselective side of the metallocene wedge to form highly isotactic polymer.

Experimental

General Considerations. All air- and moisture-sensitive compounds were manipulated using standard vacuum line, Schlenk, or cannula techniques or in a glove box under a nitrogen atmosphere, as described previously.²⁵ Dinitrogen, dihydrogen, deuterium, and argon were purified by passage over

MnO on vermiculite and activated molecular sieves. Ethereal solvents were stored over sodium benzophenone ketyl, hydrocarbon solvents were stored over titanocene, and halogenated solvents were dried over calcium hydride.²⁶ Solvents were also dried by the method of Grubbs.²⁷ Benzene-*d*₆ was distilled from LiAlH₄ and then distilled from sodium sand before use.

Tetrahydrofuran-*d*₈ was distilled from sodium benzophenone ketyl and stored over 4 Å molecular sieves. The tBuSpH₂ ligand (**7**) and its dilithio and dipotassio salts (**4** and **15**) were prepared via standard procedures.²⁸

tBuSpZr(NMe₂)₂ (**5**) was prepared following the method of Jordan from **7** and Zr(NMe₂)₄ (**6**); **6** was prepared by the method of Jordan.¹⁴ ScCl₃(THF)₃ and YCl₃(THF)_{3.5} were prepared according to literature methods.²⁹ LiCH₂CMe₃, LiCH₂SiMe₃,³⁰ and B(C₆F₅)₃³¹ were prepared according to previously reported procedures. All other reagents were purchased from Aldrich and used as received or purified using standard methods.³²

Instrumentation. Most ¹H, and ¹³C NMR spectra were recorded on a Varian Mercury 300 spectrometer at 299.868 Mhz and 75.409 MHz, respectively, at room temperature unless indicated otherwise. Some ¹H and ¹³C spectra were recorded on a Varian INOVA 500 spectrometer at 499.852 MHz, 125.669 MHz, or 76.848 MHz, respectively, at room temperature unless indicated otherwise. Nuclear Overhauser difference experiments were carried out on a Varian INOVA 500 spectrometer. All ¹H and ¹³C NMR chemical shifts are reported relative to TMS, and ¹H (residual) or ¹³C chemical shifts of the solvent are used as a secondary standard. Temperatures of the NMR probe were calibrated using a methanol standard. EPR spectra were recorded on a Bruker EMX spectrometer. X-ray crystallography was carried out by Dr. Michael W. Day and Lawrence M. Henling.

Synthesis of tBuSpZrCl₂ (1**).** *Route A.* In the glove box a round bottom flask was charged with Li₂tBuSp (4.459 g, 17 mmol, 1 equiv) and ZrCl₄ (4.053 g, 17 mmol, 1 equiv) and equipped with a reflux condenser. On the vacuum line, approximately 100 mL of toluene was added by vacuum transfer. The

apparatus was attached to the Schlenk line and refluxed for 5 days, during which time it turned a mustard yellow color. Toluene was removed *in vacuo*, and petroleum ether was added to the product by vacuum transfer. The product was stirred in petroleum ether for ten hours, petroleum was removed *in vacuo*, and the product was extracted with diethyl ether. Recrystallization of the product from diethyl ether provides 3.868 g of **1** as a yellow powder in 55% yield. *Route B.* Complex **5** (2.000 g, 4.8 mmol, 1 equiv) was placed in a round bottom flask in the glove box, and the flask was equipped with a swivel frit assembly and attached to the vacuum line. Toluene was added via vacuum transfer. Approximately 5 mL of Me₃SiCl (39 mmol, 8 equiv) was added, and the mixture was stirred for 14 hours under argon. Solvents were removed *in vacuo*, and petroleum ether was added via vacuum transfer and removed 3 times. The product was washed with petroleum ether to leave 1.118 g of **1** in 58% yield. ¹H NMR (RT, 300 MHz, C₆D₆): δ = 0.078 (s, 3H, SiCH₃), 0.20 (s, 3H, SiCH₃), 1.44 (s, 9H, C(CH₃)₃), 5.46 (m, 1H, CpH), 5.53 (m, 1H, CpH), 5.65 (m, 1H, CpH), 5.73 (m, 1H, CpH), 6.66 (m, 1H, CpH), 6.82-6.85 (m, 2H, CpH). ¹³C{¹H} NMR (RT, 500 MHz, C₆D₆): δ = -6.57, -4.63 (Si(CH₃)₂), 30.85 (C(CH₃)₃), 33.72 (C(CH₃)₃), 105.72, 107.87, 111.38, 113.70, 113.77, 117.53, 124.85, 129.55, 130.92, 150.36 (Cp).

Synthesis of tBuSpZr(CH₂SiMe₃)₂ (8**).** In the glove box a 25 mL round bottom flask was charged with **1** (0.462 g, 1.1 mmol, 1 equiv) and LiCH₂(SiMe₃) (0.215 g, 2.3 mmol, 2 equiv) and equipped with a swivel frit assembly. The apparatus was attached to the vacuum line, and approximately 15 mL of toluene was added by vacuum transfer. The reaction was allowed to stir at room temperature under argon for 14 hours. Solvent was removed *in vacuo*, petroleum ether was added and the product was extracted with petroleum ether. Recrystallization from petroleum ether provided 0.030 g of **8** as an orange powder in 5% yield. ¹H NMR (RT, 300 MHz, C₆D₆): δ = -0.43 (d, 1H, ZrCH₂Si(CH₃)₃), 0.11 (d, 1H, ZrCH₂Si(CH₃)₃), 0.20 (s, 9H, ZrCH₂Si(CH₃)₃), 0.23 (s, 9H, ZrCH₂Si(CH₃)₃), 0.26 (s, 6H, SiCH₃), 0.41 (d, 1H, ZrCH₂Si(CH₃)₃), 0.67 (d, 1H, ZrCH₂Si(CH₃)₃), 1.37 (s, 9H, C(CH₃)₃),

5.53 (m, 1H, CpH), 5.61 (m, 1H, CpH), 5.85 (m, 1H, CpH), 6.05 (m, 1H, CpH), 6.63 (m, 1H, CpH), 6.91 (m, 1H, CpH), 7.01 (m, 1H, CpH).

Synthesis of tBuSpZrMe₂ (9). *Route A.* In the glove box a 25 mL flask was charged with **1** (1.260 g, 3.1 mmol, 1 equiv) and equipped with a swivel frit assembly. The apparatus was attached to the vacuum line and approximately 15 mL of diethyl ether was added by vacuum transfer. A diethyl ether solution of methyllithium (4.78 mL, 6.7 mmol, 2.15 equiv) was added via syringe at $-78\text{ }^{\circ}\text{C}$. The reaction mixture was warmed to $0\text{ }^{\circ}\text{C}$ and left to stir under argon for 6 hours, at which point it was a tan solution with white precipitate. The mixture was filtered and washed with diethyl ether and dried under vacuum to leave an oily tan material, which turned dark brown over 14 hours. The brown oil was taken up in petroleum ether, and the product was extracted with petroleum ether. Cooling this petroleum ether solution to $-78\text{ }^{\circ}\text{C}$ caused precipitation of an off-white powder, which was filtered cold and dried to give 0.476 g of **9** in 42% yield. *Route B.* In the glove box a 50 mL round bottom flask was charged with **5** (3.500 g, 8.3 mmol, 1 equiv), and approximately 15 mL of toluene was added. A solution of AlMe₃ (2.998 g, 42 mmol, 5 equiv) in 17 mL of petroleum ether was slowly added by pipette to the toluene solution of **5**. The solution turned from a dark orange to a paler orange. The flask was equipped with a swivel frit assembly and attached to the vacuum line. The reaction mixture was cooled to $0\text{ }^{\circ}\text{C}$ and allowed to slowly warm to room temperature, and the mixture was stirred at room temperature for 5 hours. Solvents were removed *in vacuo*, petroleum ether was added via vacuum transfer to dissolve all of the orange-yellow powder, and the solution was cooled to $-78\text{ }^{\circ}\text{C}$, causing a yellow precipitate to crash out of solution. The cold solution was filtered and dried under vacuum. The yellow solid was collected and recrystallized again from cold petroleum ether to give 1.424 g of **9** as an off-white powder in 47% yield. ¹H NMR (RT, 300 MHz, C₆D₆): δ = 0.011 (s, 3H, ZrCH₃), 0.026 (s, 3H, ZrCH₃), 0.13 (s, 3H, SiCH₃), 0.21 (s, 3H, SiCH₃), 1.38 (s, 9H, C(CH₃)₃), 5.33 (m, 1H, CpH), 5.36 (m, 1H, CpH), 5.62 (m, 1H, CpH), 5.64 (m, 1H, CpH), 6.57 (m, 1H, CpH),

6.69 (m, 1H, CpH), 6.75 (m, 1H, CpH). $^{13}\text{C}\{^1\text{H}\}$ NMR (RT, 300 MHz, C_6D_6): $\delta = -6.08, -4.28$ (Si(CH₃)₂), 28.24, 31.67 (Zr(CH₃)₂), 31.34 (C(CH₃)₃), 33.40 (C(CH₃)₃), 98.44, 100.38, 110.18, 110.31, 111.84, 114.36, 119.50, 119.97, 122.09, 144.89 (Cp).

Synthesis of [tBuSpZrH₂]₂ (10). In the glove box a thick-walled bomb was charged with **9** (0.522 g, 1.4 mmol, 1 equiv). The apparatus was attached to the vacuum line and approximately 30 mL of toluene was added via vacuum transfer. The solution was cooled to $-196\text{ }^\circ\text{C}$, and the solution was placed under an atmosphere of H₂. The bomb was sealed and allowed to stir at room temperature for 14 days. During this time the flask was periodically degassed on the vacuum line to remove methane and more H₂ was added at $-196\text{ }^\circ\text{C}$. After 14 days, solvent was removed *in vacuo*, and petroleum ether was added via vacuum transfer and removed under vacuum. The apparatus was taken into the glove box, and the tan solid was taken up in petroleum ether and transferred to a 25 mL flask equipped with a swivel frit assembly. The product was extracted with petroleum ether and recrystallized from cold petroleum ether to leave 0.228 g of **10** as a white powder in 47% yield. ^1H NMR (RT, 500 MHz, C_6D_6): $\delta = -2.05$ (t, 2H, $\mu\text{-H}$), 0.19 (s, 6H, SiCH₃), 0.21 (s, 6H, SiCH₃), 1.49 (s, 18H, C(CH₃)₃), 4.13 (t, 2H, Zr-H), 5.09 (m, 1H, CpH), 5.13 (m, 1H, CpH), 5.53 (m, 1H, CpH), 5.92 (m, 1H, CpH), 6.08 (m, 1H, CpH), 6.41 (m, 1H, CpH), 7.11 (m, 1H, CpH). $^{13}\text{C}\{^1\text{H}\}$ NMR (RT, 500 MHz, C_6D_6): $\delta = -7.01, -4.12$ (Si(CH₃)₂), 32.28 (C(CH₃)₃), 32.75 (C(CH₃)₃), 91.23, 99.26, 100.82, 104.15, 106.06, 109.42, 109.50, 110.91, 112.93, 149.85 (Cp). Colorless X-ray quality crystals of **10** were obtained by cooling a saturated toluene solution of **10** to $-30\text{ }^\circ\text{C}$ for days.

Synthesis of tBuSpZrMeCl (11). *Route A.* In the glove box a 50 mL flask is charged with solid **9** (0.611 g, 1.7 mmol, 1 equiv) and solid [iPr₂NH₂]⁺Cl⁻ (0.231 g, 1.7 mmol, 1 equiv) and equipped with a swivel frit assembly. The apparatus was attached to the vacuum line, and approximately 30 mL of dichloromethane was added by vacuum transfer. The resulting pale yellow solution was allowed to stir at room temperature under an atmosphere of

argon for 20 hours, after which time solvent was removed *in vacuo*. Petroleum ether was added via vacuum transfer and removed 2 times, and the product was isolated by recrystallization from cold petroleum ether to give 0.447 g of **11** in 69% yield. *Route B*. In the glove box a bomb was charged with **1** (0.386 g, 0.95 mmol, 1 equiv) and **9** (0.347 g, 0.95 mmol, 1 equiv), attached to the vacuum line, and toluene was added by vacuum transfer. The bomb was sealed and heated to 80 °C for 5 days. The bomb was taken into the glove box, and its contents were transferred to a 25 mL flask equipped with a swivel frit assembly. Toluene was removed under vacuum, and the product was extracted with petroleum ether and recrystallized from cold petroleum ether to leave 0.421 g of **11** in 57% yield. ¹H NMR (RT, 300 MHz, C₆D₆): δ = 0.005 (s, 3H, SiCH₃, minor isomer), 0.10 (s, 3H, SiCH₃, major isomer), 0.17 (s, 3H, SiCH₃, major isomer), 0.22 (s, 3H, SiCH₃, minor isomer), 0.53 (s, 3H, ZrCH₃, major isomer), 0.56 (s, 3H, ZrCH₃, minor isomer), 1.39 (s, 9H, C(CH₃)₃, minor isomer), 1.42 (s, 9H, C(CH₃)₃, major isomer), 5.35 (m, 3H, CpH, 2H major isomer, 1H minor isomer), 5.61 (m, 3H, CpH, minor isomer), 5.70 (m, 2H, CpH, 1H major isomer, 1H minor isomer), 5.76 (m, 1H, CpH, major isomer), 6.42 (m, 1H, CpH, minor isomer), 6.61 (m, 2H, CpH, major isomer), 6.65 (m, 1H, CpH, major isomer), 6.75 (m, 1H, CpH, minor isomer). Yellow X-ray quality crystals of **11** were obtained by cooling a saturated hexanes solution of **11** to -30 °C for weeks.

Synthesis of tBuSpZrMe(CH₂CMe₃) (12). In the glove box, a 25 mL flask was charged with **11** (0.098 g, 0.26 mmol, 1 equiv) and LiCH₂CMe₃ (0.020 g, 0.26 mmol, 1 equiv) and equipped with a swivel frit assembly. The apparatus was attached to the vacuum line, and 15 mL of toluene was added by vacuum transfer. The reaction mixture was stirred at room temperature under an atmosphere of argon for 14 hours, the solvent was removed *in vacuo*, and the product was extracted with petroleum ether to leave **12** as a yellow oil. ¹H NMR (RT, 300 MHz, C₆D₆): δ = -0.40 (d, 1H, ZrCH₂C(CH₃)₃, minor isomer), 0.016 (s, 3H, ZrCH₃, major isomer), 0.045 (s, 3H, ZrCH₃, minor isomer), 0.15 (s, 3H, SiCH₃, major isomer), 0.21 (s, 3H, SiCH₃, minor isomer), 0.24 (s, 3H, SiCH₃,

major isomer), 0.26 (s, 3H, SiCH₃, minor isomer), 0.53 (d, 1H, ZrCH₂C(CH₃)₃, major isomer), 0.78 (d, 1H, ZrCH₂C(CH₃)₃, major isomer), 1.13 (s, 9H, ZrCH₂C(CH₃)₃, major isomer), 1.14 (s, 9H, ZrCH₂C(CH₃)₃, minor isomer), 1.40 (s, 9H, C(CH₃)₃, major isomer), 1.41 (s, 9H, C(CH₃)₃, minor isomer), 5.28 (m, 1H, CpH, minor isomer), 5.33 (m, 1H, CpH, minor isomer), 5.55 (m, 1H, CpH, major isomer), 5.60 (m, 2H, CpH, major isomer), 5.65 (m, 1H, CpH, major isomer), 5.84 (m, 1H, CpH, minor isomer), 6.20 (m, 1H, CpH, minor isomer), 6.49 (m, 1H, CpH, major isomer), 6.62 (m, 1H, CpH, minor isomer), 6.72 (m, 1H, CpH, minor isomer), 6.83 (m, 1H, CpH, minor isomer), 7.05 (m, 1H, CpH, major isomer), 7.13 (m, 1H, CpH, major isomer). X-ray quality crystals of **12** were obtained by cooling a saturated hexanes solution of **12** to -30 °C for weeks.

Synthesis of tBuSpZrMe(CH₂SiMe₃) (13). Complex **13** was prepared using a procedure analogous to that used to isolate **12** from **11** (0.081 g, 0.21 mmol, 1 equiv) and LiCH₂SiMe₃ (0.021 g, 0.22 mmol, 1 equiv) and isolated as a yellow oil. ¹H NMR (RT, 300 MHz, C₆D₆): δ = -0.42 (d, 1H, ZrCH₂Si(CH₃)₃, major isomer), -0.019 (s, 6H, ZrCH₃, 3H major isomer, 3H minor isomer), 0.11 (d, 1H, ZrCH₂Si(CH₃)₃, minor isomer), 0.13 (s, 3H, SiCH₃, minor isomer), 0.17 (s, 9H, ZrCH₂Si(CH₃)₃, minor isomer), 0.20 (s, 9H, ZrCH₂Si(CH₃)₃, major isomer), 0.25 (s, 9H, SiCH₃, 6H major isomer, 3H minor isomer), 0.40 (d, 1H, ZrCH₂Si(CH₃)₃, minor isomer), 0.67 (d, 1H, ZrCH₂Si(CH₃)₃, major isomer), 1.36 (s, 9H, C(CH₃)₃, major isomer), 1.38 (s, 9H, C(CH₃)₃, minor isomer), 5.27 (m, 1H, CpH, major isomer), 5.33 (m, 1H, CpH, major isomer), 5.51 (m, 1H, CpH, minor isomer), 5.56 (m, 1H, CpH, minor isomer), 5.63 (m, 1H, CpH, minor isomer), 5.67 (m, 1H, CpH, minor isomer), 5.74 (m, 1H, CpH, major isomer), 5.91 (m, 1H, CpH, major isomer), 6.47 (m, 1H, CpH, minor isomer), 6.68 (m, 1H, CpH, major isomer), 6.71 (m, 2H, CpH, major isomer), 6.91 (m, 1H, CpH, minor isomer), 6.94 (m, 1H, CpH, minor isomer). ¹³C{¹H} NMR (RT, 300 MHz, C₆D₆): δ = -6.14, -5.65, -3.83, -3.55 (SiCH₃), 3.92, 3.98 (ZrCH₂Si(CH₃)₃), 25.98, 29.52 (ZrCH₃), 31.56, 31.74 (C(CH₃)₃), 33.54, 33.66 (C(CH₃)₃), 47.51, 51.03 (ZrCH₂Si(CH₃)₃),

98.75, 99.76, 100.92, 101.99, 108.80, 109.71, 110.25, 111.23, 111.93, 112.31, 113.40, 116.02, 116.53, 118.56, 119.42, 120.66, 122.15, 122.94, 144.42, 144.54 (Cp).

Synthesis of tBuSpScCl(THF) (14). In the glove box a 25 mL flask was charged with $\text{ScCl}_3(\text{THF})_3$ (1.326 g, 3.6 mmol, 1 equiv) and **15** (1.157 g, 3.6 mmol, 1 equiv) and equipped with a swivel frit assembly. The apparatus was attached to the vacuum line and 15 mL of THF was added by vacuum transfer. The yellow solution was allowed to stir at room temperature under vacuum for 14 hours. Solvent was removed *in vacuo*, diethyl ether was added via vacuum transfer, the solution was allowed to stir for 2 hours at room temperature, and diethyl ether was removed under vacuum. Diethyl ether was added again via vacuum transfer, and the solution was filtered and washed 3 times with recycled solvent. The product was recrystallized from cold petroleum ether, and 0.569 g of **14** was isolated as an off-white powder in 40% yield. ^1H NMR (RT, 300 MHz, $\text{THF}-d_8$): $\delta = 0.63$ (s, 3H, SiCH_3), 0.72 (s, 3H, SiCH_3), 1.25 (s, 9H, $\text{C}(\text{CH}_3)_3$), 1.73 (br s, 4H, THF), 3.58 (br s, 4H, THF), 5.68 (m, 1H, CpH), 5.78 (m, 1H, CpH), 5.85 (m, 1H, CpH), 5.93 (m, 1H, CpH), 6.19 (m, 2H, CpH), 6.47 (m, 1H, CpH). Colorless X-ray quality crystals of **14** were obtained by cooling a saturated diethyl ether solution of **14** to -35°C .

Synthesis of tBuSpScCH(SiMe₃)₂ (17). In the glove box a 25 mL flask was charged with **14** (0.481 g, 1.2 mmol, 1 equiv) and $\text{LiCH}(\text{SiMe}_3)_2$ (0.248 g, 1.5 mmol, 1.25 equiv) and equipped with a swivel frit assembly. The apparatus was attached to the vacuum line and approximately 15 mL of toluene was added via vacuum transfer. The reaction was left to stir at room temperature for 14 hours, after which time solvent was removed *in vacuo*. Petroleum ether was added via vacuum transfer, and the product was extracted with petroleum ether to leave **17** as a yellow oil. ^1H NMR (RT, 300 MHz, C_6D_6): $\delta = 0.081$ (s, 9H, $\text{ScCH}(\text{Si}(\text{CH}_3)_3)_2$), 0.14 (s, 9H, $\text{ScCH}(\text{Si}(\text{CH}_3)_3)_2$), 0.51 (s, 3H, SiCH_3), 0.61 (s, 3H, SiCH_3), 1.15 (s, 9H, $\text{C}(\text{CH}_3)_3$), 1.85 (s, 1H, $\text{ScCH}(\text{Si}(\text{CH}_3)_3)_2$), 5.42 (m, 1H, CpH), 5.51 (m, 1H, CpH), 5.62 (m, 2H, CpH), 6.53 (m, 1H, CpH), 6.64 (m, 1H, CpH), 6.95 (m, 1H, CpH).

Synthesis of [tBuSpScH]_n (18). In the glove box a bomb was charged with **17**. The bomb was attached to the vacuum line and toluene was added by vacuum transfer. The bomb was exposed to an atmosphere of H₂ at -196 °C, sealed, and left to stir at room temperature for 1 week. Solvent was removed *in vacuo*, and the product was washed with pentane to leave 0.100 g of **18** as a white solid. ¹H NMR (RT, 300 MHz, C₆D₆): δ = 0.342 (s, 3H, SiCH₃), 0.482 (s, 3H, SiCH₃), 1.16 (s, 9H, C(CH₃)₃), 5.19 (m, 1H, CpH), 5.56 (m, 1H, CpH), 5.71 (m, 1H, CpH), 6.69 (m, 1H, CpH), 7.06 (m, 1H, CpH), 7.11 (m, 1H, CpH), 7.33 (m, 1H, CpH).

Synthesis of tBuSpTiCl₂ (19). In the glove box a 250 mL round bottom flask was charged with TiCl₃(THF)₃ (1.678 g, 4.5 mmol, 1 equiv) and **4** (1.161 g, 4.5 mmol, 1 equiv) and equipped with a 180 ° needle valve. The flask was attached to the vacuum line and toluene was added via vacuum transfer. The reaction mixture was stirred at room temperature for 16 hours, at which point it was taken into the glove box, and solid PbCl₂ (1.67 g, 6 mmol, 1.3 equiv) was added to the solution. The mixture was stirred for 16 hours at room temperature. The solution was filtered through celite in the glove box to remove Pb⁰, and solvent was removed from the filtrate *in vacuo*. Petroleum ether was added via vacuum transfer, and the mixture was filtered using a swivel frit and the product extracted with petroleum ether. Solvent was removed *in vacuo*, the brown powder was dissolved in CCl₄ in air. The product was isolated from an aqueous workup with aqueous HCl, followed by washing with water and brine, and drying the CCl₄ solution with MgSO₄. Compound **19** was isolated as 0.405 g of a green-brown powder in 25% yield. ¹H NMR (RT, 300 MHz, CDCl₃): δ = 0.65 (s, 3H, SiCH₃), 0.78 (s, 3H, SiCH₃), 1.41 (s, 9H, C(CH₃)₃), 5.81 (m, 1H, CpH), 5.97 (m, 1H, CpH), 6.06 (m, 1H, CpH), 6.11 (m, 1H, CpH), 7.02 (m, 1H, CpH), 7.08 (m, 1H, CpH), 7.20 (m, 1H, CpH). ¹³C{¹H} NMR (RT, 300 MHz, CDCl₃): δ = -5.80, -3.91 (SiCH₃), 30.81 (C(CH₃)₃), 34.95 (C(CH₃)₃), 103.93, 104.46, 116.51, 117.90, 119.49, 122.79, 130.44, 137.22, 137.58, 156.16 (Cp).

Characterization of tBuSpZrH₂(PMe₃) (20). In the glove box an NMR tube equipped with a Teflon valve was charged with **10** (0.009 g, 0.013 mmol, 1 equiv), and 0.7 mL of C₆D₆ was added. The NMR tube was attached to the vacuum line and PMe₃ (15.7 mL at 31.7 torr, 0.026 mmol, 2 equiv) was added via vacuum transfer. The reaction was monitored by ¹H NMR, and the equilibrium constant was determined at room temperature by integration. ¹H NMR (RT, 300 MHz, C₆D₆): δ = 0.34 (s, 3H, SiCH₃), 0.35 (s, 3H, SiCH₃), 0.98 (d, 9H, ZrP(CH₃)₃), 1.41 (s, 9H, C(CH₃)₃), 4.90 (m, 1H, CpH), 4.95 (m, 1H, CpH), 5.17 (m, 2H, CpH), 6.38 (m, 1H, CpH), 6.54 (m, 1H, CpH), 6.68 (m, 1H, CpH). ³¹P{¹H} NMR (RT, 300 MHz, C₆D₆): δ = -15.63 (ZrP(CH₃)₃).

Characterization of [tBuSpZrMe]⁺[MeB(C₆F₅)₃]⁻ (21). In the glove box an NMR tube equipped with a Teflon valve was charged with **9** (0.008 g, 0.022 mmol, 1 equiv) and B(C₆F₅)₃ (0.012 g, 0.023 mmol, 1.05 equiv) and 0.7 mL of toluene-*d*₈ was added. The reaction mixture was examined by ¹H NMR at room temperature and -20 °C to show quantitative formation of **21** as 2 isomers. The major isomer has been identified as the one in which MeB(C₆F₅)₃⁻ is *anti* to the tBu group. ¹H NMR (RT, 500 MHz, toluene-*d*₈): δ = -0.18 (s, 3H, SiCH₃, major isomer), -0.073 (s, 3H, SiCH₃, minor isomer), 0.079 (s, 3H, SiCH₃, major isomer), 0.13 (s, 3H, SiCH₃, minor isomer), 0.46 (s, 3H, ZrCH₃, major isomer), 0.49 (s, 3H, ZrCH₃, minor isomer), 0.52 (br s, 3H, CH₃B(C₆F₅)₃, minor isomer), 0.56 (br s, 3H, CH₃B(C₆F₅)₃, major isomer), 0.69 (s, 9H, C(CH₃)₃, minor isomer), 1.00 (s, 9H, C(CH₃)₃, major isomer), 5.05 (m, 1H, CpH, minor isomer), 5.11 (m, 1H, CpH, major isomer), 5.18 (m, 1H, CpH, minor isomer), 5.24 (m, 1H, CpH, major isomer), 5.31 (m, 1H, CpH, major isomer), 5.42 (m, 1H, CpH, major isomer), 5.49 (m, 2H, CpH, minor isomer), 6.30 (m, 1H, CpH, major isomer), 6.33 (m, 1H, CpH, major isomer), 6.40 (m, 1H, CpH, minor isomer), 6.41 (m, 1H, CpH, major isomer), 6.48 (m, 1H, CpH, major isomer).

Characterization of [tBuSpZrCH₂(SiMe₃)]⁺[MeB(C₆F₅)₃]⁻ (22). In the glove box an NMR tube equipped with a Teflon valve was charged with **13** (0.011 g,

0.025 mmol, 1 equiv) and $B(C_6F_5)_3$ (0.014 g, 0.027 mmol, 1.05 equiv) and 0.7 mL of toluene- d_8 was added. Above 0 °C the complex undergoes fast exchange of the anion to either side of the metallocene wedge. The reaction mixture was examined by 1H NMR at a range of temperatures (0 to -60 °C) to show quantitative formation of **22** as 2 isomers. 1H NMR (-40 °C, 500 MHz, toluene- d_8): δ = -0.13 (s, 3H, $SiCH_3$, major isomer), -0.043 (s, 9H, $ZrCH_2Si(CH_3)_3$, minor isomer), 0.0050 (s, 9H, $ZrCH_2Si(CH_3)_3$, major isomer), 0.030 (s, 3H, $SiCH_3$, major isomer), 0.045 (s, 3H, $SiCH_3$, minor isomer), 0.17 (s, 3H, $SiCH_3$, minor isomer), 0.36 (d, 1H, $ZrCH_2Si(CH_3)_3$, major isomer), 0.48 (br s, 3H, $CH_3B(C_6F_5)_3$, minor isomer), 0.60 (br s, 3H, $CH_3B(C_6F_5)_3$, major isomer), 0.80 (s, 9H, $C(CH_3)_3$, minor isomer), 0.96 (s, 9H, $C(CH_3)_3$, major isomer), 1.23 (d, 1H, $ZrCH_2Si(CH_3)_3$, minor isomer), 1.75 (d, 1H, $ZrCH_2Si(CH_3)_3$, minor isomer), 4.97 (m, 1H, CpH, minor isomer), 5.02 (m, 1H, CpH, minor isomer), 5.20 (m, 1H, CpH, major isomer), 5.37 (m, 1H, CpH, major isomer), 5.51 (m, 1H, CpH, major isomer), 5.60 (m, 1H, CpH, major isomer), 5.67 (m, 1H, CpH, minor isomer), 5.81 (m, 1H, CpH, minor isomer), 6.35 (m, 1H, CpH, major isomer), 6.44 (m, 1H, CpH, major isomer), 6.58 (m, 1H, CpH, major isomer), 6.86 (m, 1H, CpH, minor isomer), 7.15 (m, 1H, CpH, minor isomer).

Crystallography. Crystal data, intensity collection, and refinement details are presented in Tables 2 – 5 for compounds **10**, **11**, **12**, and **14**.

Data Collection and Processing. Data for compounds **10**, **11**, **12**, and **14** were collected on a CCD area detector running SMART.³³ The diffractometer was equipped with a Crystal Logic CL24 low temperature device, and all data sets were collected at 98 K. The diffractometer used graphite-monochromated $MoK\alpha$ radiation with $\lambda = 0.71073 \text{ \AA}$. The crystals were mounted on a glass fiber with Paratone-N oil. Data were collected as ω -scans at 5 to 7 ϕ settings. The detector was 5 cm (nominal) distant at a θ angle of -28°. The data were processed with SAINT.³³

Empirical Formula	$C_{32}H_{48}Si_2Zr_2 \cdot C_7H_8$
Formula Weight (g/mol)	763.46
Crystallization Solvent	Toluene
Crystal Habit	Irregular Piece
Crystal Size (mm ³)	0.40 X 0.10 X 0.10
Crystal Color	Colorless
Preliminary Photos	Rotation
Type of Diffractometer	CCD Area Detector
Wavelength	0.71073 Å MoK α
Data Collection Temperature (K)	98(2)
θ Range for 10516 Reflections Used in Lattice Determination (°)	2.30 to 27.73
Unit Cell Dimension a (Å)	11.2049(11)
Unit Cell Dimension b (Å)	12.3388(12)
Unit Cell Dimension c (Å)	14.5820(14)
α (°)	72.417(2)
β (°)	86.850(2)
γ (°)	85.018(2)
Volume (Å ³)	1913.7(3)
Z	2
Crystal System	Triclinic
Space Group	P ⁻¹
Calculated Density (Mg/m ³)	1.325
F(000)	796
Data Collection Program	Bruker SMART
θ Range for Data Collection (°)	1.47 to 28.47
Completeness to $\theta = 28.47^\circ$ (%)	91.5
Index Ranges	$-15 \leq h \leq 14, -16 \leq k \leq 16, -19 \leq l \leq 19$
Data Collection Scan Type	ω scans at 5 ϕ settings
Data Reduction Program	Bruker SAINT v6.2
Reflections Collected	28,772
Independent Reflections	8,851 ($R_{int} = 0.0621$)
Absorption Coefficient (mm ⁻¹)	0.632
Absorption Correction	None
Max. and Min. Transmission (Calculated)	0.9395 and 0.7862
Structure Solution Program	SHELXS-97 (Sheldrick, 1990)
Primary Solution Method	Direct Methods
Secondary Solution Method	Difference Fourier Map
Hydrogen Placement	Difference Fourier Map
Structure Refinement Program	SHELXL-97 (Sheldrick, 1997)
Refinement method	Full matrix least-squares on F ²
Data/Restraints/Parameters	8851/0/601
Treatment of Hydrogen Atoms	Unrestrained except for solvent methyl
Goodness-of-Fit ^a on F ²	1.175
Final R Indices ^b ($I > 2\sigma(I)$, 6284 Reflections)	R1 = 0.0383, wR2 = 0.0626

R Indices ^b (All Data)	R1 = 0.0596, wR2 = 0.0659
Type of Weighting Scheme Used	Sigma
Weighting Scheme Used	$w = 1/\sigma^2(Fo^2)$
Max Shift/Error	0.002
Average Shift/Error	0.000
Largest Diff. Peak and Hole (e/Å ³)	0.832 and -0.440

Table 2. X-ray experimental data for **10**. ^aGoodness-of-Fit (S) is based on F²; F set to zero for negative F². ^bR-factors (R) are based on F and weighted R-factors (wR) are based on F².

Empirical Formula	C ₁₇ H ₂₅ ClSiZr
Formula Weight (g/mol)	384.13
Crystallization Solvent	Hexanes
Crystal Habit	Fragment
Crystal Size (mm ³)	0.34 X 0.25 X 0.18
Crystal Color	Yellow
Preliminary Photos	Rotation
Type of Diffractometer	CCD Area Detector
Wavelength	0.71073 Å MoKα
Data Collection Temperature (K)	98(2)
θ Range for 16829 Reflections Used in Lattice Determination (°)	2.18 to 28.15
Unit Cell Dimension a (Å)	7.5776(5)
Unit Cell Dimension b (Å)	12.5670(9)
Unit Cell Dimension c (Å)	18.6149(13)
β (°)	90.3200(10)
Volume (Å ³)	1772.6(2)
Z	4
Crystal System	Monoclinic
Space Group	P2 ₁ /n
Calculated Density (Mg/m ³)	1.439
F(000)	792
Data Collection Program	Bruker SMART
θ Range for Data Collection (°)	1.96 to 28.19
Completeness to θ = 28.19° (%)	95.6
Index Ranges	-10 ≤ h ≤ 10, -16 ≤ k ≤ 16, -24 ≤ l ≤ 24
Data Collection Scan Type	ω scans at 7 φ settings
Data Reduction Program	Bruker SAINT v6.2
Reflections Collected	34,942
Independent Reflections	4,167 (R _{int} = 0.0547)
Absorption Coefficient (mm ⁻¹)	0.828
Absorption Correction	None
Max. and Min. Transmission (Calculated)	0.8632 and 0.7638

Structure Solution Program	SHELXS-97 (Sheldrick, 1990)
Primary Solution Method	Direct Methods
Secondary Solution Method	Difference Fourier Map
Hydrogen Placement	Geometric Positions
Structure Refinement Program	SHELXL-97 (Sheldrick, 1997)
Refinement method	Full matrix least-squares on F ²
Data/Restrains/Parameters	4167/0/192
Treatment of Hydrogen Atoms	Riding
Goodness-of-Fit ^a on F ²	3.764
Final R Indices ^b (I > 2σ(I), 3598 Reflections)	R1 = 0.0575, wR2 = 0.1089
R Indices ^b (All Data)	R1 = 0.0661, wR2 = 0.1093
Type of Weighting Scheme Used	Sigma
Weighting Scheme Used	w = 1/σ ² (Fo ²)
Max Shift/Error	0.000
Average Shift/Error	0.000
Largest Diff. Peak and Hole (e/Å ³)	4.112 and -1.283

Table 3. X-ray experimental data for **11**. ^aGoodness-of-Fit (S) is based on F²; F set to zero for negative F². ^bR-factors (R) are based on F and weighted R-factors (wR) are based on F².

Empirical Formula	C ₂₂ H ₃₆ SiZr
Formula Weight (g/mol)	419.82
Crystallization Solvent	Hexanes
Crystal Habit	Block
Crystal Size (mm ³)	0.20 X 0.19 X 0.13
Crystal Color	Yellow
Preliminary Photos	Rotation
Type of Diffractometer	CCD Area Detector
Wavelength	0.71073 Å MoKα
Data Collection Temperature (K)	98(2)
θ Range for 18447 Reflections Used in Lattice Determination (°)	2.14 to 28.32
Unit Cell Dimension a (Å)	7.8240(7)
Unit Cell Dimension b (Å)	28.510(3)
Unit Cell Dimension c (Å)	10.3218(10)
β (°)	111.0910(10)
Volume (Å ³)	2148.2(3)
Z	4
Crystal System	Monoclinic
Space Group	P2 ₁ /n
Calculated Density (Mg/m ³)	1.298

F(000)	888
Data Collection Program	Bruker SMART
θ Range for Data Collection ($^{\circ}$)	1.43 to 28.36
Completeness to $\theta = 28.36^{\circ}$ (%)	95.8
Index Ranges	$-10 \leq h \leq 10, -37 \leq k \leq 37, -13 \leq l \leq 13$
Data Collection Scan Type	ω scans at 7 ϕ settings
Data Reduction Program	Bruker SAINT v6.2
Reflections Collected	43,676
Independent Reflections	5,144 ($R_{\text{int}} = 0.0676$)
Absorption Coefficient (mm^{-1})	0.569
Absorption Correction	None
Max. and Min. Transmission (Calculated)	0.9297 and 0.8947
Structure Solution Program	SHELXS-97 (Sheldrick, 1990)
Primary Solution Method	Direct Methods
Secondary Solution Method	Difference Fourier Map
Hydrogen Placement	Geometric Positions
Structure Refinement Program	SHELXL-97 (Sheldrick, 1997)
Refinement method	Full matrix least-squares on F^2
Data/Restraints/Parameters	5144/0/226
Treatment of Hydrogen Atoms	Riding
Goodness-of-Fit ^a on F^2	3.212
Final R Indices ^b ($I > 2\sigma(I)$, 4392 Reflections)	$R1 = 0.0712, wR2 = 0.1010$
R Indices ^b (All Data)	$R1 = 0.0849, wR2 = 0.1019$
Type of Weighting Scheme Used	Sigma
Weighting Scheme Used	$w = 1/\sigma^2(F_o^2)$
Max Shift/Error	0.001
Average Shift/Error	0.000
Largest Diff. Peak and Hole ($e/\text{\AA}^3$)	3.937 and -2.346^c

Table 4. X-ray experimental data for **12**. ^aGoodness-of-Fit (S) is based on F^2 ; F set to zero for negative F^2 . ^bR-factors (R) are based on F and weighted R-factors (wR) are based on F^2 . ^cThe two dominant features of the final electron density Fourier map lie within 1 \AA of zirconium. All other features are less than 1 $e/\text{\AA}^3$. The diffraction peaks were very broad, and presumably the two dominant features of the map are an artifact of this.

Empirical Formula	$\text{C}_{20}\text{H}_{30}\text{ClOScSi}$
Formula Weight (g/mol)	394.94
Crystallization Solvent	Ethyl Ether
Crystal Habit	Irregular
Crystal Size (mm^3)	0.33 X 0.18 X 0.07

Crystal Color	Colorless
Preliminary Photos	Rotation
Type of Diffractometer	CCD Area Detector
Wavelength	0.71073 Å MoK α
Data Collection Temperature (K)	98(2)
θ Range for 10435 Reflections Used in Lattice Determination ($^{\circ}$)	2.34 to 27.90
Unit Cell Dimension a (Å)	16.2929(16)
Unit Cell Dimension b (Å)	10.3877(10)
Unit Cell Dimension c (Å)	12.4674(12)
β ($^{\circ}$)	104.504(2)
Volume (Å ³)	2042.8(3)
Z	4
Crystal System	Monoclinic
Space Group	P2 ₁ /n
Calculated Density (Mg/m ³)	1.284
F(000)	840
Data Collection Program	Bruker SMART
θ Range for Data Collection ($^{\circ}$)	2.35 to 28.44
Completeness to $\theta = 28.44^{\circ}$ (%)	94.1
Index Ranges	-21 \leq h \leq 21, -13 \leq k \leq 13, -16 \leq l \leq 16
Data Collection Scan Type	ω scans at 6 ϕ settings
Data Reduction Program	Bruker SAINT v6.2
Reflections Collected	34,884
Independent Reflections	4,845 ($R_{\text{int}} = 0.1064$)
Absorption Coefficient (mm ⁻¹)	0.554
Absorption Correction	None
Max. and Min. Transmission (Calculated)	0.9602 and 0.8370
Structure Solution Program	SHELXS-97 (Sheldrick, 1990)
Primary Solution Method	Patterson Method
Secondary Solution Method	Difference Fourier Map
Hydrogen Placement	Difference Fourier Map
Structure Refinement Program	SHELXL-97 (Sheldrick, 1997)
Refinement method	Full matrix least-squares on F ²
Data/Restraints/Parameters	4845/0/337
Treatment of Hydrogen Atoms	Unrestrained
Goodness-of-Fit ^a on F ²	1.429
Final R Indices ^b ($I > 2\sigma(I)$, 3544 Reflections)	R1 = 0.0407, wR2 = 0.0717
R Indices ^b (All Data)	R1 = 0.0623, wR2 = 0.0744
Type of Weighting Scheme Used	Sigma
Weighting Scheme Used	$w = 1/\sigma^2(\text{Fo}^2)$
Max Shift/Error	0.001
Average Shift/Error	0.000
Largest Diff. Peak and Hole (e/Å ³)	0.557 and -0.558

Table 5. X-ray experimental data for **14**. ^aGoodness-of-Fit (S) is based on F^2 ; F set to zero for negative F^2 . ^bR-factors (R) are based on F and weighted R-factors (wR) are based on F^2 .

Structure Analysis and Refinement. Crystallographic data for the structure of **10** (CCDC 159913) have been deposited with the Cambridge Crystallographic Data Centre (CCDC), 12 Union Road, Cambridge CB2, 1EZ, UK, and copies can be obtained on request, free of charge, by quoting the deposition number 159913. Structure factors are available electronically by e-mail: xray@caltech.edu. Crystallographic data for the structure of **11** (CCDC 171696) have been deposited with the Cambridge Crystallographic Data Centre (CCDC), 12 Union Road, Cambridge CB2, 1EZ, UK, and copies can be obtained on request, free of charge, by quoting the deposition number 171696. Structure factors are available electronically by e-mail: xray@caltech.edu. Crystallographic data for the structure of **12** (CCDC 238208) have been deposited with the Cambridge Crystallographic Data Centre (CCDC), 12 Union Road, Cambridge CB2, 1EZ, UK, and copies can be obtained on request, free of charge, by quoting the deposition number 238208. Structure factors are available electronically by e-mail: xray@caltech.edu. Crystallographic data for the structure of **14** (CCDC 160920) have been deposited with the Cambridge Crystallographic Data Centre (CCDC), 12 Union Road, Cambridge CB2, 1EZ, UK, and copies can be obtained on request, free of charge, by quoting the deposition number 160920. Structure factors are available electronically by e-mail: xray@caltech.edu.

References

- ¹ (a) Ziegler, K.; Martin, H.; Holzkamp, E.; Breil, H. DB Patent 1,268,392, 1954. (b) Ziegler, E.; Holzkamp, H.; Breil, H.; Martin, H. DB Patent 973,626, 1953. (c) Ziegler, E.; Holzkamp, H.; Breil, H.; Martin, H. DB Patent 1,257,430, 1954. (d) Natta, G.; Pino, P.; Manzanti, G. Ital. Patent 535,712, 1954.

-
- ² Brintzinger, H. H.; Fischer, D.; Mulhaupt, R.; Rieger, B.; Waymouth, R. M. *Angew. Chem. Int. Ed. Engl.* **1995**, *34*, 1143.
- ³ Association of Plastic Manufacturers in Europe, **2004**.
- ⁴ Kaminsky, W.; Kulper, K.; Brintzinger, H. H.; Wild, F. W. P. *Angew. Chem. Int. Ed. Engl.* **1985**, *24*, 507.
- ⁵ Gilchrist, J. H.; Bercaw, J. E. *J. Am. Chem. Soc.* **1996**, *118*, 12021.
- ⁶ Jordan, R. F. *Adv. Organomet. Chem.* **1991**, *32*, 325.
- ⁷ (a) Piers, W. E.; Bercaw, J. E. *J. Am. Chem. Soc.* **1990**, *112*, 9406. (b) Krauledat, H.; Brintzinger, H. H. *Angew. Chem. Int. Ed. Engl.* **1990**, *102*, 1412. (c) Grubbs, R. H.; Coates, G. W. *Acc. Chem. Res.* **1996**, *29*, 85.
- ⁸ Guerra, G.; Cavallo, L.; Moscardi, G.; Vacetello, M.; Corradini, P. *J. Am. Chem. Soc.* **1994**, *116*, 2988.
- ⁹ Pino, P.; Cioni, P.; Wei, J. *J. Am. Chem. Soc.* **1987**, *109*, 6189.
- ¹⁰ Pino, P.; Galimberti, M. *J. Organomet. Chem.* **1989**, *370*, 1.
- ¹¹ Gilchrist, J. H.; Bercaw, J. E. *J. Am. Chem. Soc.* **1996**, *118*, 12021.
- ¹² (a) Mise, T.; Miya, S.; Yamazaki, H. *Chem. Lett.* **1989**, 1853. (b) Zhong, H. A. *Ph.D. Thesis*, California Institute of Technology, **2001**.
- ¹³ (a) Doherty, N. M.; Bercaw, J. E. *J. Am. Chem. Soc.* **1985**, *107*, 2670. (b) Burger, B. J.; Santarsiero, B. D.; Trimmer, M. S.; Bercaw, J. E. *J. Am. Chem. Soc.* **1988**, *110*, 3134. (c) Chirik, P. J.; Zubris, D. L.; Ackerman, L. J.; Henling, L. M.; Day, M. W.; Bercaw, J. E. *Organometallics* **2003**, *22*, 172. (d) Ackerman, L. J.; Green, M. L. H.; Green, J. C.; Bercaw, J. E. *Organometallics* **2003**, *22*, 188.
- ¹⁴ Diamond, G. M.; Jordan, R. F.; Petersen, J. L. *J. Am. Chem. Soc.* **1996**, *118*, 8024.
- ¹⁵ Chirik, P. J.; Day, M. W.; Bercaw, J. E. *Organometallics* **1999**, *18*, 1873.
- ¹⁶ (a) Jones, S. B.; Petersen, J. L. *Inorg. Chem.* **1981**, *20*, 2889. (b) Lee, H.; Desrosiers, P. J.; Guzei, I.; Rheingold, A. L.; Parkin, G. J. *J. Am. Chem. Soc.* **1998**, *120*, 3255. (c) Choukroun, R.; Dahan, F.; Larssonneur, A.-M.; Samuel, E.; Petersen, J.; Meunier, P.; Sornay, C. *Organometallics* **1991**, *10*, 374. (d) Chirik, P. J.; Henling, L. M.; Bercaw, J. E. *Organometallics* **2001**, *20*, 534.
- ¹⁷ A search of the Cambridge Crystallographic Database for $(R_nCp)Zr(R)Cl$ complexes gave average M-C distances of 2.24 – 2.40 Å.

-
- ¹⁸ Hunter, W. E.; Hrcncir, D. C.; Bynum, R. V.; Penttila, R. A.; Atwood, J. L. *Organometallics* **1983**, *2*, 750.
- ¹⁹ A search of the Cambridge Crystallographic Database for $(R_nCp)Zr(R)Cl$ complexes gave average Zr-Cl distances of 2.42-2.57 Å.
- ²⁰ A search of the Cambridge Crystallographic Database for $(R_nCp)Zr(R)Np$ complexes gave average Zr-C distances of 2.16-2.48 Å.
- ²¹ Champion, B. K.; Heyn, R. H.; Tilley, T. D. *Organometallics* **1993**, *12*, 2584.
- ²² (a) Stern, D.; Sabat, M.; Marks, T. J. *J. Am. Chem. Soc.* **1990**, *112*, 9558. (b) Coughlin, E. B.; Henling, L. M.; Bercaw, J. E. *Inorg. Chimica Acta* **1996**, *242*, 205.
- ²³ Yoder, J. C.; Day, M. W.; Bercaw, J. E. *Organometallics* **1998**, *17*, 4946.
- ²⁴ (a) Deck, P. A.; Marks, T. J. *J. Am. Chem. Soc.* **1995**, *117*, 6128. (b) Wendt, O. F.; Bercaw, J. E. Unpublished results.
- ²⁵ Burger, B. J.; Bercaw, J. E. in *Experimental Organometallic Chemistry*; ACS Symposium Series No. 357; Wayda, A. L.; Darensbourg, M. Y. Eds.; American Chemical Society: Washington, D.C. 1987; Ch. 4.
- ²⁶ Marvich, R. H.; Brintzinger, H. H. *J. Am. Chem. Soc.* **1971**, *93*, 203.
- ²⁷ Pangborn, A. B.; Giardello, M. A.; Grubbs, R. H.; Rosen, R. K.; Timmers, F. J. *Organometallics* **1996**, *15*, 1518.
- ²⁸ Herzog, T. A. *Ph.D. Thesis*, California Institute of Technology, **1997**.
- ²⁹ Manzer, L. E. *Inorg. Synth.* **1982**, *21*, 135.
- ³⁰ Negishi, E.; Swanson, D. R.; Rousset, C. J. *J. Org. Chem.* **1990**, *55*, 5406.
- ³¹ Massey, A. G.; Park, A. J. *J. Organomet. Chem.* **1964**, *2*, 245.
- ³² Perrin, D. D.; Armagreggo, W. L. F. *Purification of Laboratory Chemicals*, 3rd ed.; Pergamon Press: New York, NY, 1988.
- ³³ Bruker (1999) SMART, SAINT, and SHELXTL. Bruker AXS Inc., Madison, Wisconsin, USA.